SOILS AND FOUNDATIONS Vol. 47, No. 2, 265–283, Apr. 2007
Japanese Geotechnical Society

VISCOUS BEHAVIOUR OF GEOGRIDS; EXPERIMENT AND SIMULATION

W. KONGKITKUL[i], DAIKI HIRAKAWA[ii] and FUMIO TATSUOKA[iii]

ABSTRACT

The viscous properties of three types of geogrid polymer were evaluated by sustained loading tests lasting for 30 days at a load level about a half of its nominal rupture strength. The sustained loading tests were performed during otherwise monotonic loading (ML) at constant strain or load rate, unlike the conventional creep tests, in which the strain rate immediately before the start of sustained loading, which controls the creep strain rate, is not controlled or even not recorded. The following are presented in this study. The tensile rupture strength measured by ML that was started following a 30 day-long sustained loading was essentially the same as the one at the same strain rate at rupture obtained by continuous ML without any intermission of sustained loading. This fact indicates that creep is not a degrading phenomenon. Then, if free from chemical and mechanical degrading effects, the strength of a geosynthetic reinforcement (for a given strain rate at rupture) can be maintained until late in its service life. A non-linear three-component model is used to simulate the experimental results from the previous and present studies. The model can simulate very well not only the load-strain behaviour during ML with and without step changes in the strain rate and the one after sustained loading, but also the time histories of creep strain during sustained loading for short (one hour) and long (30 days) periods.

Key words: creep, geogrid, geosynthetic reinforcement, non-linear three-component model, rupture strength, simulation, strain rate, sustained loading, tensile loading test, viscous property (**IGC**: D6/M9)

INTRODUCTION

The tensile deformation and strength characteristics of polymer geosynthetic reinforcement are more-or-less rate-dependent due to its viscous property (e.g., Bush, 1986; Bathurst and Cai, 1994; Min et al., 1995; Leshchinsky et al., 1997; Hirakawa et al., 2002, 2003; Kongkitkul et al., 2002, 2004a, b, c; Tatsuoka et al., 2004; Shinoda and Bathurst, 2004a, b). Creep deformation is defined as the deformation that takes place at constant load. In the current design procedure, the design tensile strength at the end of a specified design life time of a given polymer geosynthetic reinforcement type is obtained by reducing a short-term tensile strength obtained by monotonic loading (ML) at a relatively high strain rate using a relatively large creep reduction factor. The creep reduction factor is obtained based on the so-called "stress-rupture curve" (i.e., the relationship between the sustained tensile load and the logarithm of the period until creep rupture since the start of constant load application), as illustrated in Fig. 1 (Greenwood, 1994). The stress-rupture curve is obtained by performing a set of conventional creep rupture tests. The period until creep rupture becomes generally shorter with an increase in the load level. As the conventional creep rupture tests are significantly time-consuming, Thornton et al. (1998) proposed a method called "Stepped Isothermal Method (SIM)" to reduce the time to rupture by step increasing the temperature of environment surrounding the test specimen.

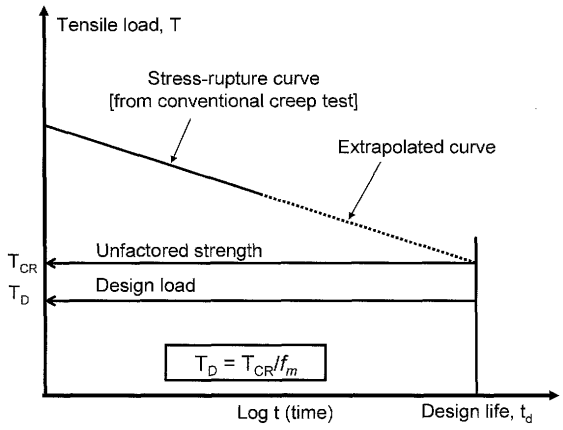

Fig. 1. Conventional creep rupture curve, after Greenwood (1994)

When following this current design procedure, the design tensile strength always decreases with an increase

[i] Postdoctoral Fellow, Department of Civil Engineering, Tokyo University of Science, Japan (formerly Graduate Student, University of Tokyo, Japan).
[ii] Research Associate, ditto.
[iii] Professor, ditto (tatsuoka@rs.noda.tus.ac.jp).
The manuscript for this paper was received for review on January 24, 2006; approved on November 17, 2006.
Written discussions on this paper should be submitted before November 1, 2007 to the Japanese Geotechnical Society, 4-38-2, Sengoku, Bunkyo-ku, Tokyo 112-0011, Japan. Upon request the closing date may be extended one month.

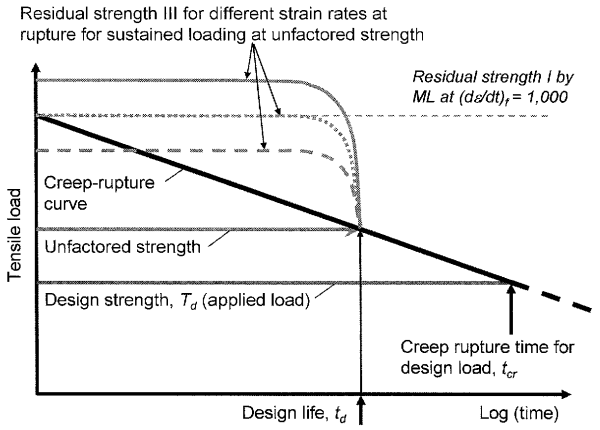

Fig. 2. Effects of strain rate at rupture on residual strength, after Tatsuoka et al. (2004)

in the design life time. The original objective of this design procedure is to remove the possibility of creep rupture failure and its implication is that, as the time to creep tensile rupture increases with a decrease in the sustained load level, a smaller design strength should be used for a longer design life time. As pointed out by Tatsuoka et al. (2004), however, this design method has the following two major drawbacks:

1) The current design method is quite misleading towards a wrong notion that creep is a degrading phenomenon. A typical misunderstanding aspect is that, even when the strength and deformation characteristics of a given polymer geosynthetic reinforcement do not physically and chemically degrade with time, the tensile strength for the same loading condition (e.g., ML at the same constant strain rate) decreases with time. However, the rupture strength is basically a function of strain rate at rupture while pre-rupture creep deformation does not noticeably affect the tensile rupture strength (e.g., Voskamp et al., 2001; Greenwood et al., 2001; Hirakawa et al., 2002, 2003; Kongkitkul et al., 2002, 2004a, b, c; Tatsuoka et al., 2004; Shinoda and Bathurst, 2004a, b). Based on the fact that creep is not a degrading phenomenon, Greenwood et al. (2001) and Tatsuoka et al. (2004) suggested a new design procedure in which the residual or available strength of a polymer geosynthetic reinforcement is a function of strain rate at rupture, not elapsed time, Fig. 2. That is, unless the material property degrades with time by physical or chemical effects, the original strength of a geosynthetic reinforcement (for a given strain rate at rupture) is maintained until late in its service life. This new proposal (Fig. 2) is no doubt much more relevant than the conventional method (Fig. 1) to seismic design, in which the structure is assumed to be subjected to seismic load after some long service period at constant boundary load.
2) In the current design method, it is assumed that the tensile load working in polymer geosynthetic reinforcement is kept constant under long-term fixed static boundary conditions. On the other hand, Tatsuoka et al. (2004) suggested that the tensile load in the polymer geosynthetic reinforcement placed in typical field full-scale backfill subjected to constant load may decrease with time due to interactions between the viscous properties of both reinforcement and backfill. Then, it is unlikely with typical full-scale geosynthetic-reinforced soil structures that the tensile rupture of polymer geosynthetic reinforcement by sustained loading becomes imminent during its life time. Therefore, the assumption that constant tensile load is maintained in the reinforcement during the whole design life is usually conservative (Kongkitkul et al., 2005).

Due to these two drawbacks, the conventional design method (Fig. 1) is likely to be largely conservative in particular with geosynthetic-reinforced soil structures designed and constructed as permanent critical structures having a sufficiently high seismic stability.

The current design methodology is implicitly and explicitly linked to the isochronous concept, which states that the present tensile load acting in given polymer geosynthetic reinforcement is a unique function of instantaneous strain and elapsed time since the start of loading. Hirakawa et al. (2002, 2003), Kongkitkul et al. (2002, 2004a, b, c) and Tatsuoka et al. (2004) showed that the isochronous concept is not able to predict and explain the load-strain behaviour of given geosynthetic reinforcement for general arbitrary loading histories, in particular the one after ML is restarted toward ultimate rupture following a long period of sustained loading. They also showed that the present tensile load in given polymer geosynthetic reinforcement is a unique function of instantaneous irreversible (or inelastic or visco-plastic) strain and its rate in the ML case, where the irreversible strain rate is always positive (i.e., tensile). Moreover, they reported the results from a comprehensive series of tensile tests on a number of different types of polymer geosynthetic reinforcement in which the strain rate was changed stepwise many times and several sustained loading and load relaxation tests were performed during otherwise ML at a constant strain rate. They showed that the test results can be well simulated by the non-linear three-component model proposed by Di Benedetto et al. (2002) and Tatsuoka et al. (2002).

In the previous studies of the authors described above, the longest period of sustained loading performed during otherwise ML at a constant strain rate was one hour, which is certainly very short when compared with usual design life time for full-scale structures. In the present study, the same geogrid types of polyester, polyarylate and polyvinyl alcohol geogrids as used previously by Hirakawa et al. (2003) were subjected to sustained loading for 30 days during otherwise ML at a constant nominal strain or load rate. A number of sustained loading tests on polymer geosynthetic reinforcement for much longer periods have been performed by other researchers (e.g., Bernardi and Paulson, 1997; Voskamp et al., 2001; Onodera et al., 2004). However, these tests were performed by load control, not during otherwise ML at a

constant strain or load rate. Moreover, the ultimate rupture strength was subsequently evaluated by ML that was started after having fully unloaded the specimen from the sustained load. For these reasons, effects on the initial strain or load rate were not critically evaluated, and the effects of long sustained loading on the load-strain behaviour and rupture strength observed during subsequent ML were not critically evaluated. In the present study, on the other hand, a sustained loading stage for 30 days was started directly following ML at a constant strain or load rate, and following the sustained loading stage, ML was restarted at the original constant strain or load rate toward tensile rupture or up to a certain load level. In the present study, the conclusions previously obtained by the authors based on results from tensile tests with relatively short sustained loading tests on polyester geogrid, as described above, was reconfirmed based on results from the newly performed tensile tests with 30 day-long sustained loading. The results from both the newly performed tests and those performed by Hirakawa et al. (2002, 2003) were simulated using the parameters obtained from the present study.

TEST MATERIAL

The following three types of polymer geogrid that were used by Hirakawa et al. (2003) and Kongkitkul et al. (2004a) were also used in the present study.

Polyester (PET): This type of geogrid has a centre-to-centre spacing of 9 mm in both longitudinal and transverse directions, coated with PVC resin for UV protection. This geogrid type is relatively weak when compared with those usually used in the construction of full-scale prototype geosynthetic-reinforced soil (GRS) structures. This type has been used in a number of scaled-down model tests because of its suitability in the similitude (e.g., Shinoda et al., 2002, 2003; Hirakawa et al., 2002).

Polyarylate: It consists of polyarylate and polyester fibres in, respectively, the longitudinal and transverse directions, also coated with PVC for UV protection with a centre-to-centre spacing between two adjacent members of 20 mm in both directions. This type of geogrid is one of the major geosynthetic reinforcement types used in the construction of GRS retaining walls in Japan.

Polyvinyl alcohol (PVA): It consists of polyvinyl alcohol fibres in both longitudinal and transverse directions, coated with PVC. Similar to polyarylate geogrid, the centre-to-centre spacing between two adjacent members is 20 mm in both directions.

The specimen of the PET geogrid consisted of five strands while those of polyarylate and PVA geogrids consisted of three strands. Regardless to the type of reinforcement tested, each specimen had a total initial length of about 900 mm with an initial unconfined length of 240 mm. To evaluate the viscous property of these geogrids, Hirakawa et al. (2003) performed displacement-controlled tests, while Kongkitkul et al. (2004a) performed load-controlled loading tests.

TEST APPARATUS

A displacement-controlled tensile loading apparatus with a capacity of 50 kN (Hirakawa et al., 2003) was used. It consists of a precise gear system with practically no backlash upon load reversal and a computer-controlled servo-motor (Tatsuoka et al., 1994; Santucci de Magistris et al., 1999). By using this loading system, it is possible: a) to smoothly switch the loading mode between displacement and load control phases and among sustained loading, load relaxation and monotonic loading or unloading; b) to change the strain rate stepwise or gradually by a factor of up to 3,000; and c) to apply small strain amplitude cyclic loading to evaluate the equivalent elastic property at any arbitrary moment. This kind of displacement-controlled loading system was used only with polyester geogrid in the present study.

A set of tensile loading tests on the polyarylate and PVA geogrids was performed by using a newly assembled load-controlled loading apparatus with a capacity of about 4 kN. The tensile load was provided by controlling the air pressure in the lower room of a double-action air cylinder arranged at the top of reaction frame. The load and load rate were controlled by means of an electro-pneumatic transducer (EP). In particular, a sustained loading test lasting for 30 days was performed during otherwise ML at a constant load rate controlling the load history before the start of sustained loading while measuring the subsequent stress-strain behaviour including the ultimate rupture strength. A report of such long-term continuous loading tests as this cannot be found in the literature.

The same gripping device was used with all the geogrids. The gripping device has a pair of roller-clamps, each consisting of a steel cylinder having a smooth surface with a groove made to grip a specimen with a small steel rod (diameter = 20 mm), Fig. 3. A sheet of sand paper was firmly glued on the surface of the clamp where a specimen was wrapped around to prevent any slippage during a test. Tensile strains over the central part with an initial gauge length of 50 mm were measured locally by using a pair of laser displacement transducers. With a single target located at the middle between those transducers, two laser displacement transducers, instead of a single, were able to measure local strains accurately. This is because, during performing a tensile loading test, the target might rotate largely around the horizontal axis, resulting in significant errors in axial strains measured with a single transducer. The tensile load was measured with an axial load cell as shown in Fig. 3. All the tests were conducted at 25 ± 2°C in a temperature-controlled laboratory.

TEST RESULTS AND DISCUSSIONS

Creep Deformation as a Viscous Response

In order to adequately evaluate the viscous property of polymer geosynthetic reinforcement and to develop its constitutive model incorporating the viscous property,

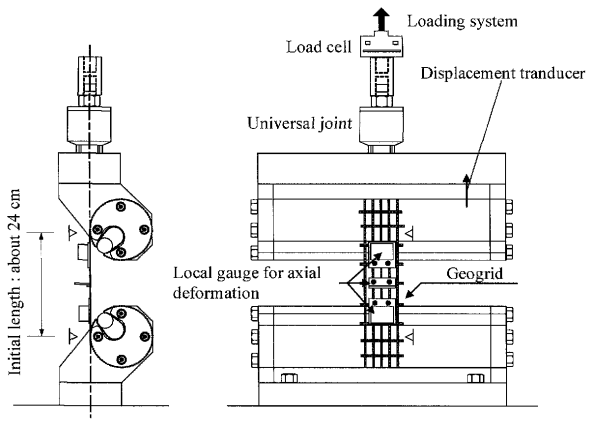

Fig. 3(a). Tensile loading apparatus with a pair of roller-clamps and a specimen, after Hirakawa et al. (2003)

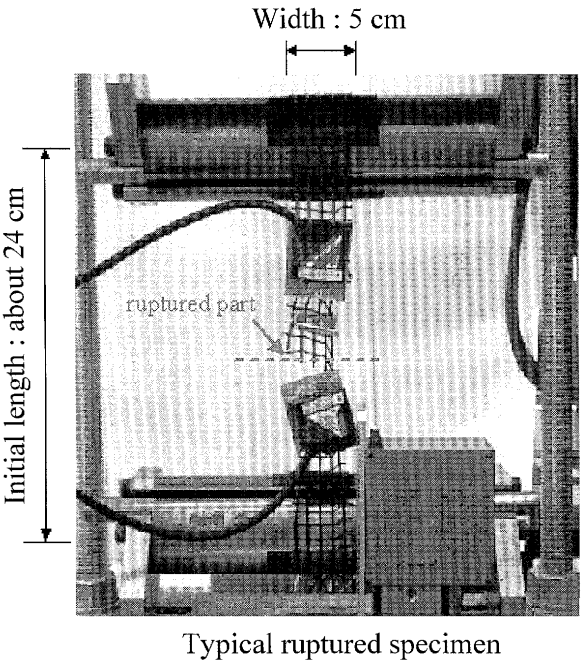

Fig. 3(b). A typical ruptured PET geogrid specimen, Hirakawa et al. (2003)

Hirakawa et al. (2003) performed a comprehensive series of tensile tests on a number of different polymer geosynthetic reinforcement types using the following loading schemes:

a) continuous ML at different but constant strain rates towards ultimate rupture;
b) sustained loading (SL) during otherwise primary ML as well as unloading and reloading at a constant strain rate;
c) several times of stepwise change in the strain rate and a set of sustained loading and load relaxation (RX) applied during otherwise ML at a constant strain rate; and
d) a number of unload/reload cycles with a double strain amplitude of the order of 0.05% to evaluate the elastic property applied during otherwise ML at a constant strain rate.

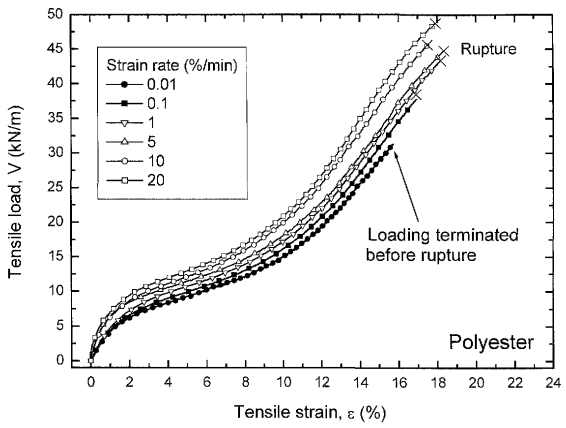

Fig. 4. Tensile load-tensile strain relations from continuous ML at different constant strain rates, PET geogrid, after Hirakawa et al. (2003)

With respect to loading scheme *b*, it should be emphasised that it is necessary to perform sustained loading tests with a known initial strain rate, unlike the conventional creep tests, to properly interpret results from sustained loading tests. To this end, it is relevant to perform sustained loading tests during otherwise monotonic loading at a known strain rate.

Figure 4 shows the relationships between the tensile load, V and the tensile strain, ε, for PET geogrid from loading scheme a), while Figs. 5(a) and 5(b) show the results from loading scheme b): i.e., sustained loading tests at three different load levels, equal to 25%, 50% and 75% of the ultimate strength when strain rate $\dot{\varepsilon}=1.0\%/$min were applied during otherwise ML at $\dot{\varepsilon}=0.1$ or $1.0\%/$min. Each sustained loading lasted for one hour. Part of the test results presented in Figs. 4 and 5(b) are also presented in Figs. 7(a) and 7(b). Figure 6 summarises the rupture strengths for PET geogrid, plotted against the logarithm of $\dot{\varepsilon}$ at rupture, from the test results presented in Figs. 4 and 5 and others obtained for more complicated loading histories (i.e., loading schemes c and d), including those presented in Figs. 7(a) and 15(a).

Figure 7(a) shows the V-ε relations from the following newly performed tests on PET geogrid:

a) a continuous ML test at a constant strain rate, $\dot{\varepsilon}$, equal to 1.0%/min toward ultimate rupture; and
b) another ML test with sustained loading that lasted for 30 days at a load level of about a half of the rupture strength from continuous ML at $\dot{\varepsilon}=1.0\%/$min.

In this figure, the result from another continuous ML test at $\dot{\varepsilon}=1.0\%/$min performed by Hirakawa et al. (2003) is also plotted. Figure 7(b) compares the V-ε relation from the ML test with 30 day-long sustained loading, presented in Fig. 7(a), and another ML test at $\dot{\varepsilon}=1.0\%/$min with multi-stage sustained loading stages lasting for one hour per stage performed by Hirakawa et al. (2003) (presented in Fig. 5(b)). It may be seen that the load-strain curves and rupture strengths under similar test conditions from the present study and Hirakawa et al. (2003) are consistent with each other, showing an acceptable

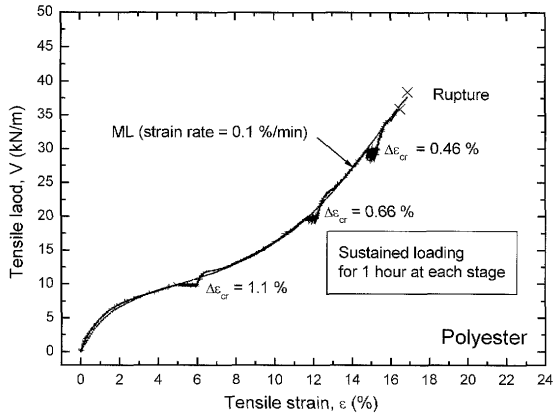

Fig. 5(a). Tensile load-strain relation during sustained loading otherwise ML at a constant strain rate of 0.1%/min, PET geogrid, after Hirakawa et al. (2003)

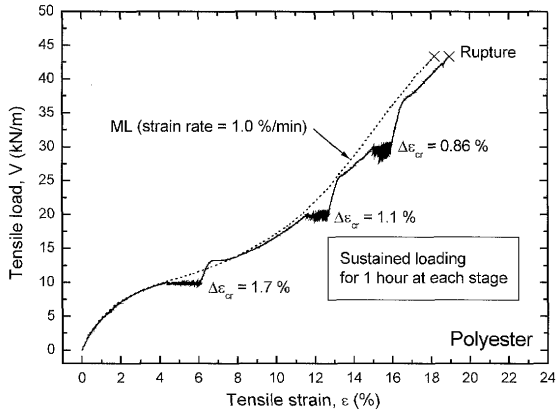

Fig. 5(b). Tensile load-strain relation during sustained loading otherwise ML at a constant strain rate of 1.0%/min, PET geogrid, after Hirakawa et al. (2003)

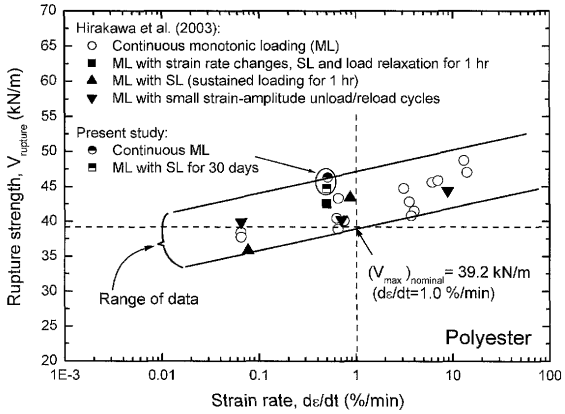

Fig. 6. Rupture strength as a function of strain rate at rupture, PET geogrid

reproducibility of test. However, a small but noticeable discrepancy can be seen between the two sets of data, which might be due to an inevitable variance in the material property among different specimens of the same product.

The following trends in behaviour can be clearly seen

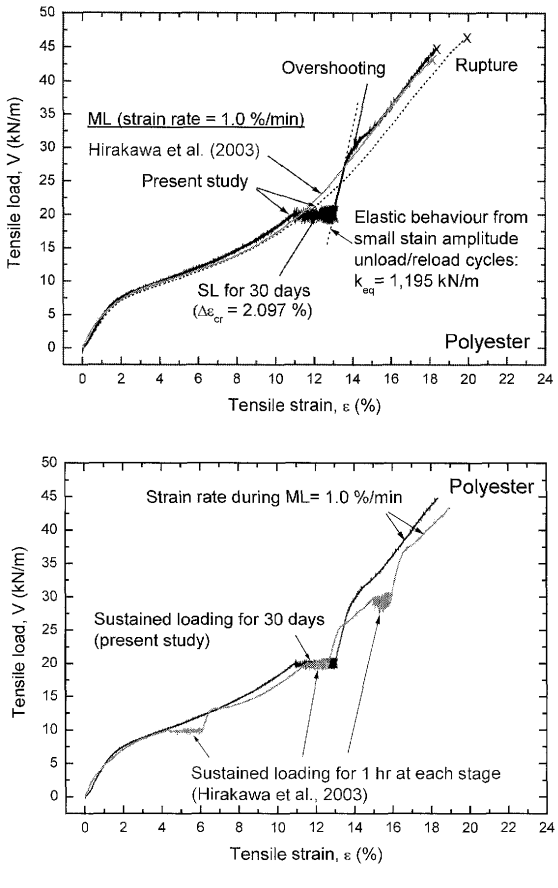

Fig. 7. Comparison of tensile load—tensile strain relations from the present study and those from Hirakawa et al. (2003), PET geogrid

from Figs. 4 through 7:

1) The pre-peak stiffness increases significantly with an increase in the strain rate, $\dot{\varepsilon}$ (Fig. 4). The rupture strength increases proportionally with the logarithm of $\dot{\varepsilon}$ at rupture, independent of pre-rupture loading histories (Fig. 6). This fact indicates that the time that has elapsed until rupture has no direct link to the rupture strength, showing that the isochronous concept is not relevant.
2) Noticeable creep deformation takes place at the respective sustained loading stage. The creep strain increment that develops for a given period of sustained loading at a given load level increases with an increase in the strain rate during ML immediately before the start of sustained loading (Figs. 5(a) and 5(b)). This result shows that the precise control of the initial creep strain rate is important when evaluating the creep strain rate history. This result also shows that creep deformation of a given prototype GRS structure would be overestimated when predicted without taking into account this factor while based on results from conventional creep tests in which the initial creep strain rate is much higher than the one with the prototype structure.
3) For a given period of sustained loading with a given initial creep strain rate, the creep strain decreases with an increase in the sustained loading level

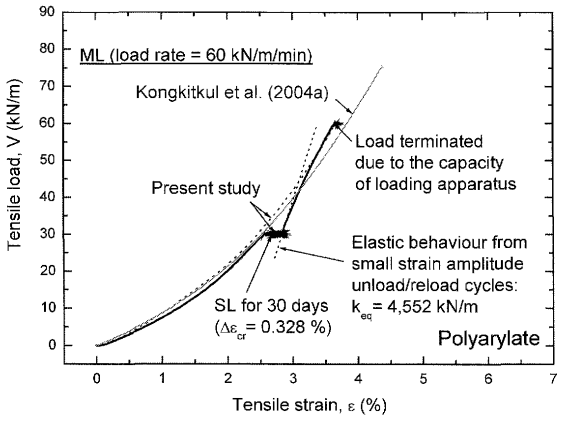

Fig. 8. Comparison of tensile load—tensile strain relations from the present study and those from Kongkitkul et al. (2004a), polyarylate geogrid

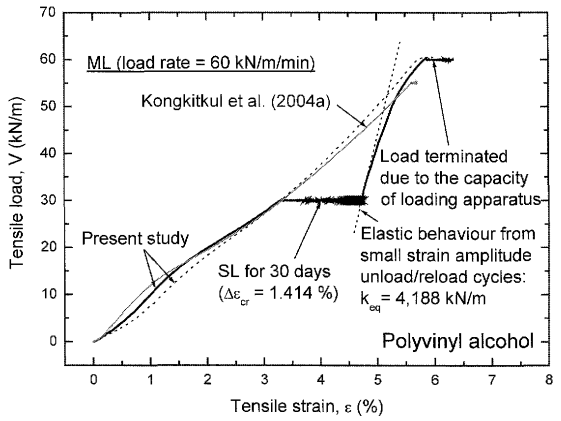

Fig. 9. Comparison of tensile load—tensile strain relations from the present study and those from Kongkitkul et al. (2004a), PVA geogrid

(Figs. 5(a) and 5(b)). This peculiar behaviour is due to such a specific feature of tensile load-tensile strain relation that the tangent stiffness increases with an increase in the load level after the load exceeds some level while before it becomes close to the peak load. The non-linear three-component model can simulate this peculiar trend of creep behaviour, as shown later in this paper.

4) For the same strain rate during ML immediately before the start of sustained loading (i.e., 1.0%/min) at the same load level (i.e., 50% of the ultimate strength at $\dot{\varepsilon}$=1.0%/min), the creep strain for a period of 30 days of PET geogrid (i.e., 2.1%) is not significantly larger than the one for one hour (i.e., 1.1%) (Fig. 7(b)).

5) When ML is restarted following the respective sustained loading stage, the tensile load-tensile strain relation exhibits a very high tangent stiffness when compared with the one observed at the same load level during continuous ML without any intermission of sustained loading (e.g., Figs. 7(a) and 7(b)). Then, the load-strain relation exhibits a noticeable load-overshooting and then clear yielding. Subsequently, the tensile load-tensile strain curve tends to rejoin the one observed during continuous ML, without showing any effects of previous sustained loading history on the subsequent load-strain behaviour. It is important to note that essentially the same trend of behaviour was observed for different strain rates during ML immediately before the start of sustained loading (i.e., 0.1 and 1.0%/min) and different periods of sustained loading (i.e., one hour and 30 days). The fact described above indicates that, regardless of sustained loading period, creep has no degrading effects on the strength and deformation characteristics observed during subsequent loading history but it is a viscous response of the polymer geosynthetic reinforcement.

Figures 8 and 9 show the V-ε relations for, respectively, polyarylate and PVA geogrids from: a) a ML test at a constant load rate, $\dot{V}$, equal to 60 kN/m/min; and b) another ML test with sustained loading that lasted for 30 days at the tensile load of 30 kN/m, both from the present study. In these figures, the results from the respective continuous ML tests at $\dot{V}$=60 kN/m/min performed by Kongkitkul et al. (2004a) are also plotted. In the present study using the load-controlled system, tensile loading was terminated at a tensile load of 60 kN/m, which is slightly lower than the capacity of the loading system. Consequently, it was decided to perform sustained loading test at the half of this load level (i.e., 30 kN/m). In Figs. 8 and 9, only slight data discrepancy can be seen within the present study and between the present study and Kongkitkul et al. (2004a). It is important to note that essentially the same trend of behaviour was observed for the different materials tested (i.e., PET, polyarylate and PVA geogrids). One different trend is that, unlike PET geogrid, when ML was restarted following the end of 30 day-long sustained loading, polyarylate and PVA geogrids exhibited no noticeably load-overshooting before rejoining the load-strain curve from continuous ML at the same load rate.

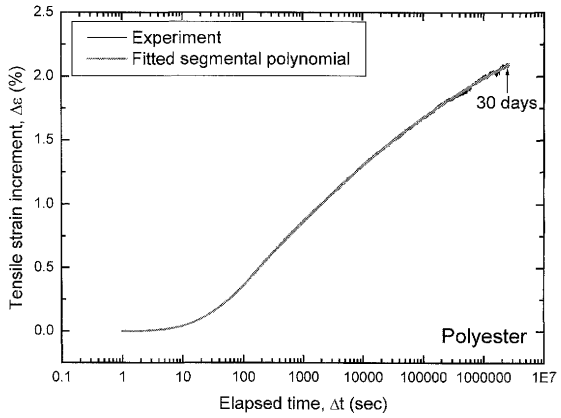

Fig. 10. Time history of creep strain increment during sustained loading for 30 days (semi-log plot), PET geogrid

Strain History during Sustained Loading for 30 Days

Figure 10 shows the time history in the logarithm time

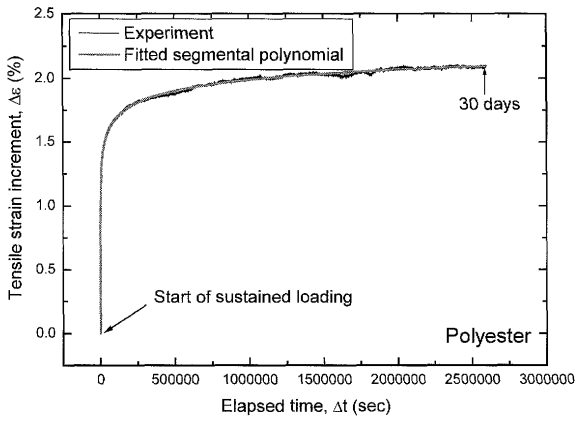

Fig. 11(a). Time history of creep strain increment during sustained loading for 30 days (in arithmetic scale), PET geogrid

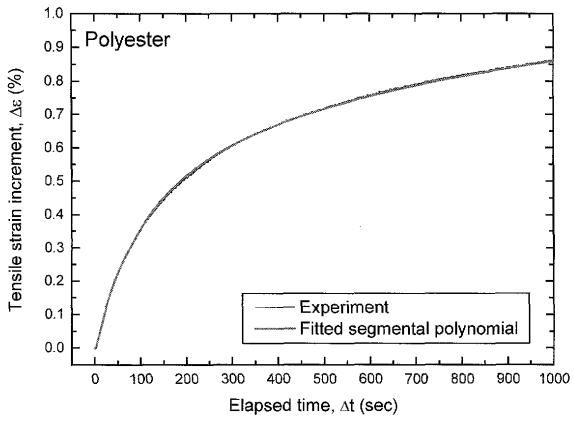

Fig. 11(c). Enlargement of Fig. 11(a) for elapsed time from 0 to 1,000 seconds, PET geogrid

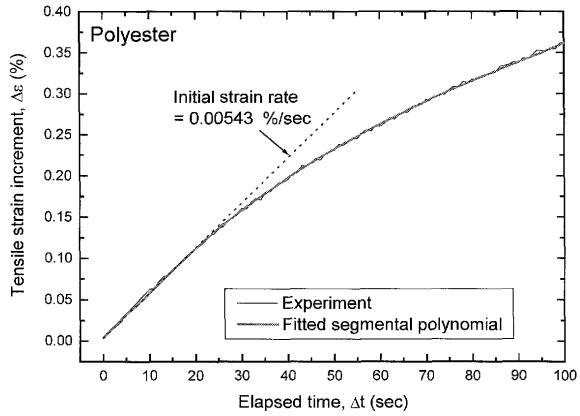

Fig. 11(b). Enlargement of Fig. 11(a) for elapsed time from 0 to 100 seconds, PET geogrid

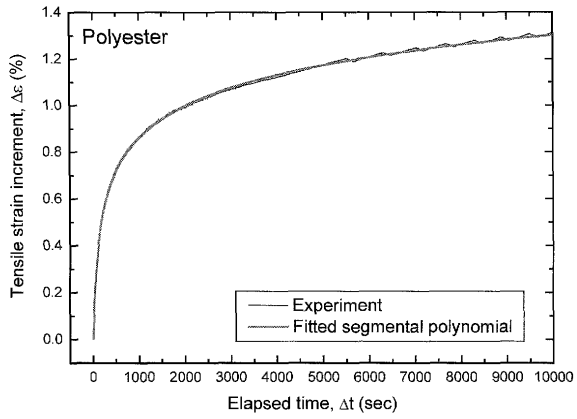

Fig. 11(d). Enlargement of Fig. 11(a) for elapsed time from 0 to 10,000 seconds, PET geogrid

scale of creep strain since the start of sustained loading for 30 days for the PET geogrid. Figures 11(a) through (d) show the same data with creep strain plotted against the elapsed time in different arithmetic time scales. Figures 12 and 13 show similar plots for polyarylate and PVA geogrids. The following trends of behaviour may be seen from Figs. 10 through 13:

1) With PET geogrid, the creep strain increment for the first one hour is equal to 1.1% (Fig. 11(d)), which is nearly the same as the value observed at the same elapsed time in the test performed under the same test conditions by Hirakawa et al. (2003) (Fig. 5(b)). This fact also shows a high repeatability of test.
2) The creep strain is not proportional to the period of sustained loading, Δt, because of a continuous decrease in the creep strain rate with time. With PET geogrid, for example, about 50% and about 80% of the total creep strain observed at $\Delta t = 30$ days have already taken place at $\Delta t =$ one hour and one day, respectively. The measured initial creep strain rate for PET geogrid at the start of the 30 day-long sustained loading is 0.00543%/sec = 0.326%/min., which is only slightly smaller than the measured irreversible strain rate during the continuous ML immediately before the start of sustained loading, equal to 0.00738%/sec. This value was obtained as the total strain rate, $\dot{\varepsilon} = 0.646\%/\text{min.} = 0.01076\%/\text{sec}$ minus the elastic strain rate, $\dot{\varepsilon}^e = \dot{V}/k_{eq}$, where $\dot{V}$ is the tensile load rate ($= 0.02368$ kN/m/sec) and k_{eq} is the instantaneous elastic stiffness, which is equal to 700 kN/m = 7 kN/m/% at the load level during the sustained loading (about a half of the rupture strength) (Hirakawa et al., 2003; Kongkitkul et al., 2004a). It should be noted that the measured strain rate, $\dot{\varepsilon}$, obtained from a tensile test is always smaller than the given nominal strain rate, which is equal to 1.0%/min in the present case (i.e., $0.646 < 1.0\%/\text{min.}$).
3) The creep strain rate at an elapsed time of 30 days was not zero but very low, regardless to different types of polymer geogrid tested (e.g., about 0.0000033%/min for PET geogrid).

The direct derivative of the measured creep strain with respect to time to obtain the history of strain rate for the whole range of the sustained loading test resulted in a large scatter. This is due to a high sensitivity of the derivative to a small scatter in the measured creep strain. Therefore, the measured time history of creep strain was fitted by an empirical equation. It was not possible to find a single function that can be fitted to the whole history of

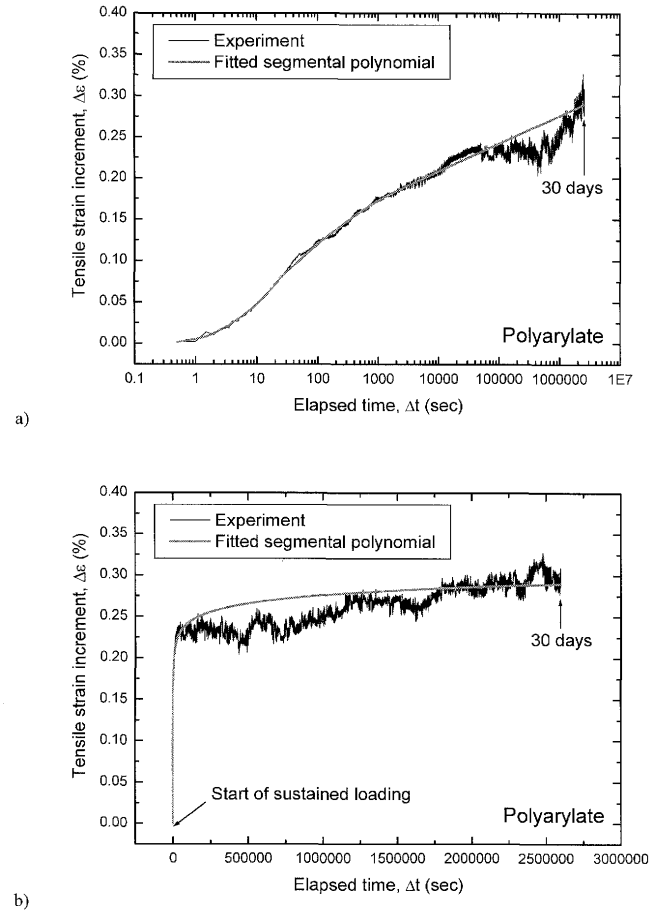

Fig. 12. Time history of creep strain increment during sustained loading for 30 days presented in: a) semi-log scale and b) arithmetic scale, polyarylate geogrid

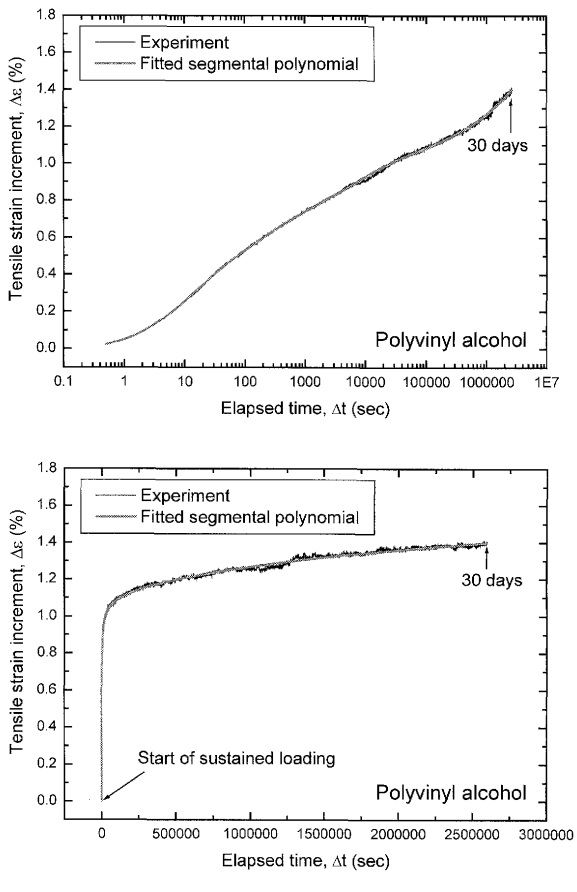

Fig. 13. Time history of creep strain increment during sustained loading for 30 days presented in: a) semi-log scale and b) arithmetic scale, PVA geogrid

Table 1. List of the constants used in Eq. (1) for each segment of time history of creep strain, PET geogrid

Segment No.	Range of elapsed time (sec)	A	B	C	D
1	$0<\Delta t\leq 10$	−7.80E-04	−1.18E-03	6.59E-03	3.96E-02
2	$10<\Delta t\leq 100$	1.57E-01	−3.71E-01	2.77E-01	−2.10E-02
3	$100<\Delta t\leq 10000$	−1.05E+00	8.89E-01	−1.10E-01	8.75E-03
4	$10000<\Delta t\leq 2592000$	−4.37E-01	4.37E-01	1.02E-02	−2.60E-03

creep strain providing a reliable time history of creep strain rate for the whole range of sustained loading. For this reason, a segmental polynomial fitting method was implemented. That is, the observed time history was separated into three or four consecutive segments and they were fitted by the respective three or four different equations in the following three-degree polynomial form:

$$\varepsilon = A + B\cdot\log(\Delta t) + C\cdot[\log(\Delta t)]^2 + D\cdot[\log(\Delta t)]^3 \quad (1)$$

where ε = creep strain increment (%); Δt = elapsed time (sec); and A, B, C and D = constants for each segment of time history, as listed in Tables 1, 2 and 3 for PET, polyarylate and PVA geogrids, respectively. The strain rate at a given Δt is obtained as:

$$\frac{d\varepsilon}{dt} = \frac{B}{\ln 10}\cdot\frac{1}{\Delta t} + \frac{2C}{(\ln 10)^2}\cdot\frac{\ln(\Delta t)}{\Delta t} + \frac{3D}{(\ln 10)^3}\cdot\frac{[\ln(\Delta t)]^2}{\Delta t} \quad (2)$$

Figures 10 through 13 show the results of this fitting procedure. It may be seen that the whole time history of measured creep strain for the respective type of reinforcements is fitted very well by this segmental polynomial fitting method.

Figures 14(a), (b) and (c) show the time histories of creep strain rate in a full-log plot obtained from the test results obtained by Eq. (2), presented in Figs. 10 through 13. Some small kinks seen on the above relation are transitions from one fitted segmental of time history to the next segment. It may be seen that, except for the initial part (e.g., when Δt is shorter than about 100 seconds with

Table 2. List of the constants used in Eq. (1) for each segment of time history of creep strain, polyarylate geogrid

Segment No.	Range of elapsed time (sec)	A	B	C	D
1	$0<\Delta t\leq 26$	2.95E-03	2.65E-02	1.20E-02	6.02E-03
2	$26<\Delta t\leq 2500$	−2.50E-02	7.87E-02	−9.68E-04	−1.11E-03
3	$2500<\Delta t\leq 2592000$	7.30E-02	3.38E-02	0	0

Table 3. List of the constants used in Eq. (1) for each segment of time history of creep strain, PVA geogrid

Segment No.	Range of elapsed time (sec)	A	B	C	D
1	$0<\Delta t\leq 10$	4.75E-02	1.17E-01	1.09E-01	−2.04E-02
2	$10<\Delta t\leq 100$	−6.32E-02	3.23E-01	6.27E-03	−9.60E-03
3	$100<\Delta t\leq 10000$	−7.51E-02	3.87E-01	−4.93E-02	3.60E-03
4	$10000<\Delta t\leq 2592000$	−3.45E+00	2.52E+00	−4.92E-01	3.38E-02

Table 4. Creep strain increments for different periods of sustained loading

Material	A=until one hour	B=between one hour and 30 days	Until 30 days		E=between 30 days and 50 years	F=between one hour and 50 years	Until 50 years	
			$C=A+B$	D			$G=D+E$	$H=A+F$
PET	1.1% (measured)	0.981% (predicted)	2.081%	2.097% (measured)	0.584% (predicted)	1.565% (predicted)	2.681%	2.665%
Polyarylate	0.194% (measured)	0.099% (predicted)	0.293%	0.328% (measured)	0.089% (predicted)	0.188% (predicted)	0.417%	0.382%
Polyvinyl alcohol	0.837% (measured)	0.381% (predicted)	1.218%	1.414% (measured)	0.218% (predicted)	0.599% (predicted)	1.632%	1.436%

PET geogrid), the creep strain rate decreases with an increase in Δt rather linearly in a full-log plot. The empirical logarithmic equations fitted to the linear part are presented in these figures. When based on these empirical equations, with PET geogrid, the creep strain at $\Delta t=30$ days predicted from the one at $\Delta t=$one hour (i.e., 1.1%; column A in Table 4) is equal to: 1.1% (at $\Delta t=$one hour)+0.981% (calculated for $\Delta t=$one hour to 30 days; column B in Table 4)=2.081% (column C in Table 4). Similar analysis with polyarylate and PVA geogrids are also listed in Table 4. These predicted values (column C) are nearly the same as the respective measured values (column D in Table 4), which validates this empirical logarithmic equation.

The total creep strain increments that would be observed at $\Delta t=50$ years were inferred by extrapolating these empirical relations from $\Delta t=30$ days to 50 years; i.e., with PET geogrid, 2.097% (measured value at $\Delta t=$ 30 days; column D)+0.584% (inferred increment for Δt =30 days to 50 years, column E)=2.681% (column G). Similar analysis with polyarylate and PVA geogrids are also listed in Table 4. This result suggests that about 78% of the total creep strain at $\Delta t=50$ years takes place for the first 30 days with PET geogrid; which is about 79% with polyarylate geogrid and 87% PVA geogrid. This analysis indicates that an elapsed time of 30 days may be sufficient to confidently predict the creep strain at $\Delta t=50$ years.

Moreover, the total creep strain increments that would be observed at $\Delta t=50$ years were inferred by extrapolating these empirical relations from $\Delta t=$one hour to 50 years; i.e., with PET geogrid, 1.1% (measured value at $\Delta t=$one hour; column A)+1.565% (inferred increment for $\Delta t=$one hour to 50 years; column F)=2.665% (column H). Again, similar analysis with polyarylate and PVA geogrids are also listed in Table 4. These total creep strains inferred based on the values measured at $\Delta t=$one hour are very similar to those inferred based on the values measured at $\Delta t=30$ days. This result indicates that an approximate total creep strain for a long period of Δt in typical field full-scale cases can be obtained from a sustained loading test for a relatively short duration; say one hour when such a logarithmic empirical equation as shown in Figs. 14(a), (b) and (c) can be defined.

The use of the empirical logarithmic creep equation presented in Fig. 14 in the analysis shown above does not mean that this equation can be applied directly to other general loading conditions (e.g., sustained loading at different load levels; sustained loading starting at other initial strain or load rates; ML at varying strain or load rates histories; and so on). To predict the load-strain-time behaviour for such general loading histories, a more general approach based on a validated constitutive model is necessary, as shown in the next section.

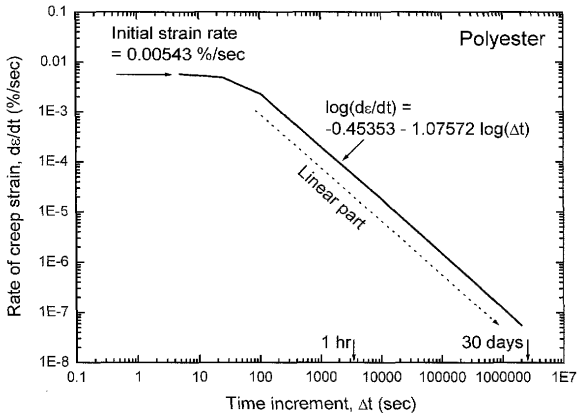

a)

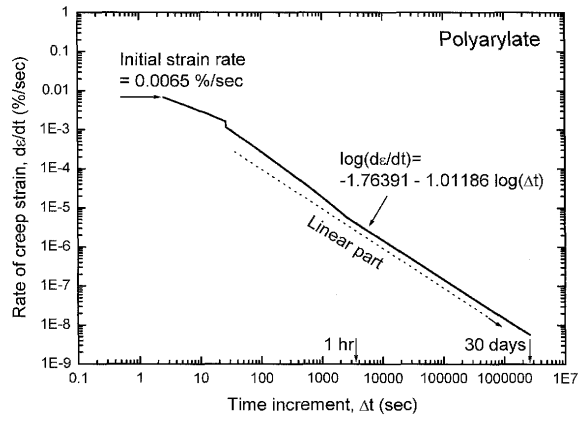

b)

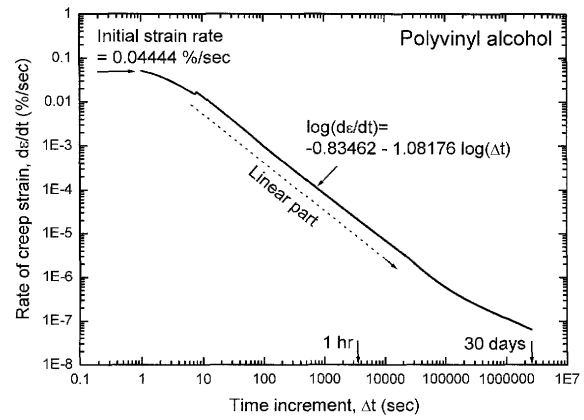

c)

Fig. 14. Relationship between creep strain rate and elapsed time from the fitted time history of creep strain increment during sustained loading for 30 days (full-log plot) for: a) PET, b) polyarylate and c) PVA geogrids

Quantification of Viscosity

To quantify the viscous property of polymer geosynthetic reinforcement, Hirakawa et al. (2003) performed a series of tensile tests with stepwise changes in the strain rate, $\dot{\varepsilon}$, and sustained loading and load relaxation stages, as typically presented in Fig. 15(a). The respective relationships between the tensile load, V, and the three types of strain (i.e., measured strain ε, irreversible strain ε^{ir} and elastic strain ε^{e}, where $\varepsilon = \varepsilon^{ir} + \varepsilon^{e}$) are presented in Fig. 15(b). In so doing, ε^{e} for a given value of V was obtained as $\int_{V=0}^{V} d\varepsilon^{e} = \int_{V=0}^{V} dV/k_{eq}(V)$, where $k_{eq}(V)$ is the

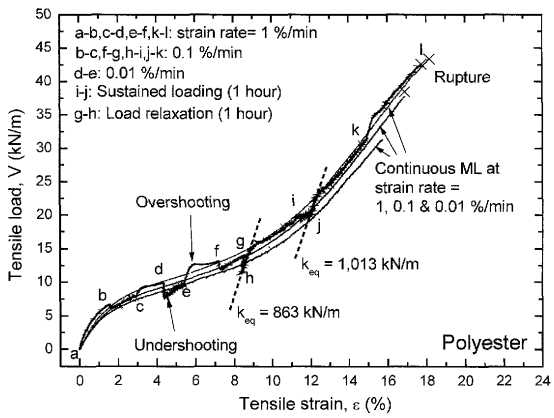

Fig. 15(a). Strain rate effects on the tensile load-tensile strain behaviour and the rupture strength, PET geogrid, after Hirakawa et al. (2003)

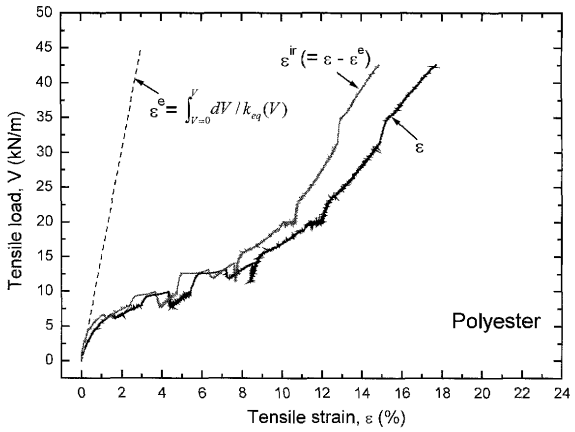

Fig. 15(b). Relationships between tensile load and three types of strain (ε, ε^{ir} and ε^{e}) from the data presented in Fig. 15(a)

equivalent elastic stiffness as a function of V determined by performing a series of small strain-amplitude unload/reload tests (Hirakawa et al., 2003; Kongkitkul et al., 2004a).

The following trends of behaviour may be seen from the test result of PET geogrid:

1) The tensile load exhibits a sudden increase/decrease upon a stepwise increase/decrease in $\dot{\varepsilon}$ by a factor ranging from 1/100 to 100. The amount of load jump, ΔV, defined in Fig. 16, upon a stepwise change in the irreversible strain rate, $\dot{\varepsilon}^{ir}$, represents the viscous property of the test material.
2) The tensile load-tensile strain curve exhibits a noticeable load-overshooting upon a step increase in $\dot{\varepsilon}$ during otherwise ML or upon the restart of ML at a constant $\dot{\varepsilon}$ following a sustained loading or load relaxation stage. On the other hand, a phenomenon of load-undershooting takes place upon a step decrease in $\dot{\varepsilon}$ during otherwise ML. It may further be seen from Fig. 15 that, as far as ML continues at a constant $\dot{\varepsilon}$ after a step change in $\dot{\varepsilon}$, the load jump decays with an increase in the strain after load-overshooting or undershooting. Such decay behaviour as described above is implemented by introducing a

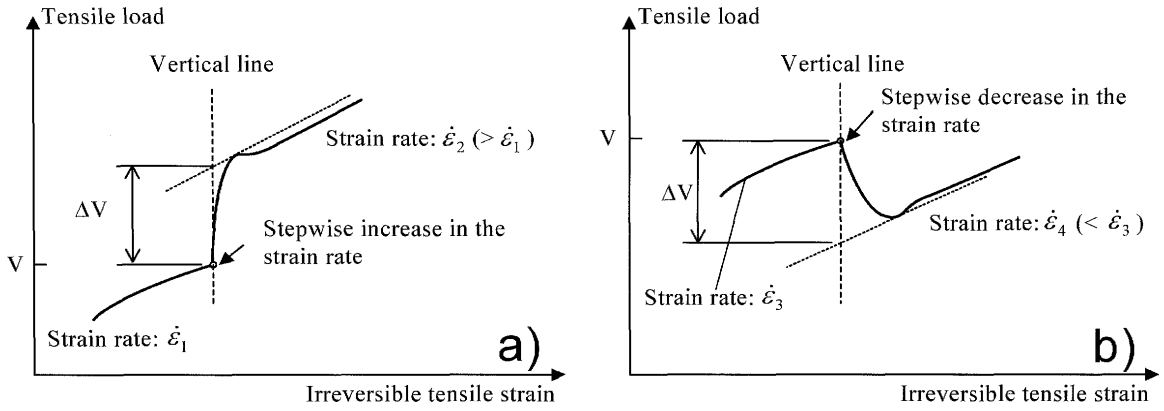

Fig. 16. Definition of tensile load jump by a stepwise increase or decrease in the irreversible strain rate, after Hirakawa et al. (2003)

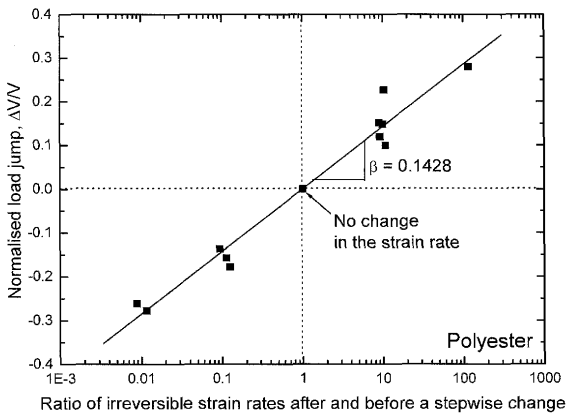

Fig. 17. Relationship between the normalised load jump and the ratio of irreversible strain rates after and before a step change, PET geogrid

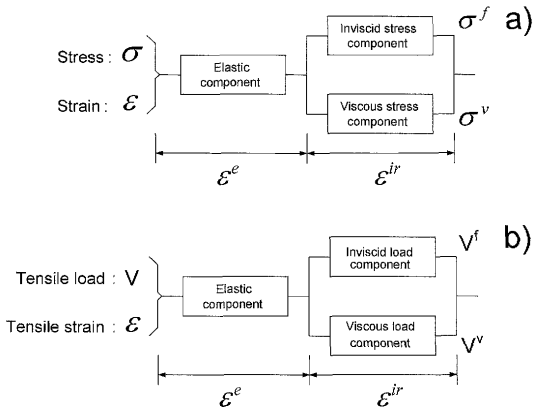

Fig. 18. a) Non-linear three-component rheology model developed for geomaterial and b) non-linear three-component model modified for polymer geosynthetic reinforcement

decay function in the non-linear three-component model as described later in this paper. Note that such load-overshooting or undershooting and subsequent decay behaviours were not observed for polyarylate and PVA geogrids (Hirakawa et al., 2003).

As the load jump per unit width, ΔV, observed for a given ratio of the irreversible strain rates after and before a given step change, $(\dot{\varepsilon}^{ir})_{after}/(\dot{\varepsilon}^{ir})_{before}$, is always proportional to the instantaneous tensile load per unit width, V, the measured ratios $\Delta V/V$ were plotted against $\log\{(\dot{\varepsilon}^{ir})_{after}/(\dot{\varepsilon}^{ir})_{before}\}$ from the data presented in Fig. 15, as shown in Fig. 17. The following linear relation may be seen:

$$\Delta V/V = \beta \cdot \log\{(\dot{\varepsilon}^{ir})_{after}/(\dot{\varepsilon}^{ir})_{before}\} \quad (3)$$

where the slope β is called "the rate-sensitivity coefficient" (Di Benedetto et al., 2005; Tatsuoka, 2005), which represents the viscous property of the test material and is linked to the model parameters of the non-linear three-component model, as explained in the next section. The β value for the data presented in Fig. 17 is equal to 0.1428. Hirakawa et al. (2003) and Kongkitkul et al. (2004a) reported the β values of a number of different types of polymer geosynthetic reinforcement. The range of these β values is relatively small (between 0.0665 and 0.1595).

SIMULATION

Non-linear Three-component Model

To simulate the load-strain-time behaviour of polymer geosynthetic reinforcement when subjected to arbitrary loading histories, the non-linear three-component model that was originally proposed to simulate the rate-dependent stress-strain behaviour of geomaterial (i.e., soil and rock) (Di Benedetto et al., 2002; Tatsuoka et al., 2002), illustrated in Fig. 18(a), was modified: i.e., the stress, σ, was replaced with the tensile load per unit width, V, Fig. 18(b). It is very important to note that the non-linear three-component model can predict the tensile load-strain-time of geosynthetic reinforcement when subjected to arbitrary loading histories and therefore it can be incorporated into a FEM code (e.g., Tatsuoka et al., 2004; Siddiquee et al., 2006). In the discussions that follow, ageing effects are not taken into account. According to the model, the tensile load, V, is given as follows in the ML case (in which $\dot{\varepsilon}^{ir}$ is always positive):

$$V = V^f(\varepsilon^{ir}) + V^v(\varepsilon^{ir}, \dot{\varepsilon}^{ir}, h_s) \quad (4)$$

where $V^f(\varepsilon^{ir})$ is the inviscid load component which is a

unique function of ε^{ir}. The $V^f(\varepsilon^{ir})$-ε^{ir} relation, which is called the reference relation, is defined as the V-ε^{ir} relation when $\dot{\varepsilon}^{ir}=0$. In the present study, the reference relation for the tested material was inferred by extrapolating the measured V-ε^{ir} relations from ML at different constant strain rates, as shown in Fig. 4. It was confirmed that the inferred reference relation is consistent with the ultimate V-ε^{ir} states that would be reached after infinitive long sustained loading obtained by extrapolating the results from the sustained loading tests for 30 days, as shown later in Figs. 25(a), 26(a) and 27(a). Moreover, Hirakawa et al. (2003) showed that the reference relation inferred as above is consistent with the trends of behaviour that are observed in sustained loading tests that start during otherwise unloading from the primary loading scheme. That is, the creep strain rate becomes positive, zero and negative when sustained loading is started from a V and ε^{ir} state that is located, respectively, above, at and below the reference relation that is inferred as above. The location where $\dot{\varepsilon}^{ir}=0$ when starting sustained loading should be located on the reference relation. Then, the reference relation was fitted by the following polynomial equation:

$$V^f=\sum_{i=1}^{10} a_i\cdot(\varepsilon^{ir})^{i-1} \tag{5}$$

where a_i is the coefficient for term i. $V^v(\varepsilon^{ir}, \dot{\varepsilon}^{ir}, h_s)$ is the viscous load component that is a function of the current irreversible strain, ε^{ir}; the current irreversible strain rate, $\dot{\varepsilon}^{ir}$; and the strain history parameter, h_s (explained later). As ΔV in Eq. (3) is defined as the change in V solely by a change in $\dot{\varepsilon}^{ir}$ at a constant ε^{ir}, we have $\Delta V^f=0$ and then Eq. (3) is rewritten as:

$$\Delta V^v/V=\beta\cdot\log\{(\dot{\varepsilon}^{ir})_{after}/(\dot{\varepsilon}^{ir})_{before}\} \tag{6}$$

Equation (6) means that the viscous load component, V^v, changes in a non-linear manner by changes in the irreversible strain rate, unlike the Newtonian type viscosity, for which the linear relation: $V^v=\eta\cdot\dot{\varepsilon}^{ir}$ (η=constant) is assumed. The following four types of V^v have been found relevant for different types of material, including a number of different types of polymer geosynthetic reinforcement (Hirakawa et al., 2003; Kongkitkul et al., 2004a). All the discussions below refer to the ML case.

Isotach viscosity: This is defined as the material viscosity when the current value of V^v is a unique function of irreversible tensile strain, ε^{ir}, and its rate, $\dot{\varepsilon}^{ir}$. So, the strain history parameter h_s for $V^v(\varepsilon^{ir}, \dot{\varepsilon}^{ir}, h_s)$ becomes unnecessary. Therefore, the change of $V^v=V^v(\varepsilon^{ir}, \dot{\varepsilon}^{ir})$ upon a change in $\dot{\varepsilon}^{ir}$ is persistent as long as ML continues at the same $\dot{\varepsilon}^{ir}$. As a result, the tensile load-tensile strain curves in ML at different constant strain rates are separated from each other. The separation increases in proportion to V^f with an increase in ε^{ir}, as the load jump, ΔV, upon a step change in $\dot{\varepsilon}^{ir}$ is always proportional to the instantaneous value of V in the experiment (Hirakawa et al., 2003; Kongkitkul et al., 2004a). Then, $V^v(\varepsilon^{ir}, \dot{\varepsilon}^{ir})$ can be written as follows:

$$V^v(\varepsilon^{ir}, \dot{\varepsilon}^{ir})=V^f(\varepsilon^{ir})\cdot g_v(\dot{\varepsilon}^{ir}) \tag{7}$$

where $g_v(\dot{\varepsilon}^{ir})$ is the viscosity function, for which the following non-linear function has been proposed for geomaterial (Di Benedetto et al., 2002; Tatsuoka et al., 1999, 2002):

$$g_v(\dot{\varepsilon}^{ir})=g_{v1}(\dot{\varepsilon}^{ir})=\alpha\cdot[1-\exp\{1-(|\dot{\varepsilon}^{ir}|/\dot{\varepsilon}^{ir}_r+1)^m\}] \tag{8}$$

where $|\dot{\varepsilon}^{ir}|$ is the absolute value of $\dot{\varepsilon}^{ir}$; α, m and $\dot{\varepsilon}^{ir}_r$ are the positive material constants. Note that the function $g_v(\dot{\varepsilon}^{ir})$ is always positive whether loading, unloading, reloading or so (i.e., irrespective of the sign of $\dot{\varepsilon}^{ir}$). On the other hand, Di Benedetto et al. (1999) chose the following another function for $g_v(\dot{\varepsilon}^{ir})$:

$$g_v(\dot{\varepsilon}^{ir})=g_{v2}(\dot{\varepsilon}^{ir})=\alpha^*\cdot(\dot{\varepsilon}^{ir}/\dot{\varepsilon}^{ir}_0)^{1+b^*} \tag{9}$$

where: α^*, b^* and $\dot{\varepsilon}^{ir}_0$ are constants. It can be shown that Eqs. (8) and (9) provide nearly the same evolutions for a wide range of positive value of $\dot{\varepsilon}^{ir}$, while the differences become noticeable only at very small or very large values of $\dot{\varepsilon}^{ir}$.

Hirakawa et al. (2003) and Kongkitkul et al. (2004a) used Eq. (8) to simulate results from the tensile loading tests in which the encountered range of $\dot{\varepsilon}^{ir}$ was not very large. On the other hand, the range of $\dot{\varepsilon}^{ir}$ that was encountered in the 30 day-long sustained loading tests (i.e., Fig. 14) was much larger: e.g., the creep deformation of PET geogrid continued while the $\dot{\varepsilon}^{ir}$ value was decreasing from an initial value of 0.00543%/sec down to 5.5×10^{-8}%/sec at an elapsed time of 30 days. As shown later, it was found that it becomes necessary to combine Eqs. (8) and (9) in such that Eq. (8) is fitted to both of the data when the $\dot{\varepsilon}^{ir}$ values are relatively high, as did by Hirakawa et al. (2003) and Kongkitkul et al. (2004a), and Eq. (9) when the $\dot{\varepsilon}^{ir}$ values are relatively low. Note that the use of only Eq. (8) is still sufficient when simulating the creep deformation for a much shorter duration. Note that the same viscosity function can also be used for the other types of viscosity explained below and the discussions on the viscosity function given above are also relevant to the other types of viscosity.

Hirakawa et al. (2003) and Kongkitkul et al. (2004a) showed that, except for the PET geogrid, the viscous property of all the other types of geosynthetic reinforcements that they tested, including the polyarylate and PVA geogrids used in the present study, can be modelled by the isotach viscosity.

TESRA viscosity: When the material viscosity is of this type, the increment of V^v, dV^v, that takes place by an increment of ε^{ir} or $\dot{\varepsilon}^{ir}$ or both increments decays with an increase in ε^{ir} when ML continues at the constant $\dot{\varepsilon}^{ir}$. A trend of such a decay dV^v may be seen in the test result presented in Fig. 15(a) (typically during sections *d-e* and *e-f*). Then, the current value of V^v becomes a function of not only ε^{ir} and $\dot{\varepsilon}^{ir}$ but also recent strain history even in the case of ML. So, V^v cannot be represented by an explicit function of ε^{ir} and $\dot{\varepsilon}^{ir}$, therefore, the strain history parameter h_s for $V^v(\varepsilon^{ir}, \dot{\varepsilon}^{ir}, h_s)$ becomes necessary. Due to the decay of dV^v, the tensile load-tensile strain relations

for ML at different constant strain rates tend to collapse into a single relation (i.e., the reference relation, Eq. (5)), in particular when approaching the peak stress state. The trend of behaviour has been observed in drained plane strain compression tests on Hostun sand (Matsushita et al., 1999) and in drained triaxial compression tests on silica No. 8 sand (Kiyota and Tatsuoka, 2006). The decay behaviour of V^v is called the TESRA viscosity (n.b., TESRA stands for Temporary Effects of Strain Rate and strain Acceleration). The TESRA viscosity is represented as:

$$V^v = V^v_{TESRA}(\varepsilon^{ir}, \dot{\varepsilon}^{ir}, h_s) = \int_{\tau=\varepsilon_1^{ir}}^{\varepsilon^{ir}} [dV^v_{iso}]_{(\tau)} \cdot r_1^{(\varepsilon^{ir}-\tau)} \quad (10)$$

where ε^{ir} is the current irreversible strain, ε_1^{ir} is the irreversible strain at the start of loading where the viscous effect is zero ($\varepsilon_1^{ir}=0$ in the present case); V^v_{iso} is the isotach viscous load component obtained from Eq. (7); and τ is the irreversible strain at which the viscous load increment $[dV^v_{iso}]_{(\tau)}$ takes place. The function $r_1^{(\varepsilon^{ir}-\tau)}$ is called the decay function. As r_1 is a positive constant lower than unity, $r_1^{(\varepsilon^{ir}-\tau)}$ decreases with an increase in the strain difference, $\varepsilon^{ir}-\tau$. In this way, the current value of V^v_{TESRA} (when $\varepsilon^{ir}=\varepsilon^{ir}$) becomes dependent of the recent history of ε^{ir}. When $r_1=1.0$, V^v_{TESRA} (Eq. (10)) becomes the same as V^v_{iso} (Eq. (7)).

General TESRA viscosity: Similar to the TESRA type viscosity, the change of V^v upon a change in $\dot{\varepsilon}^{ir}$ decays with ε^{ir}, but the decay rate increases with an increase in ε^{ir}, changing the viscosity type from the isotach type at small strains towards the TESRA type at large strains. To realistically simulate this trend of viscous property, the following expression becomes necessary:

$$V^v = V^v_{G.TESRA} = \int_{\tau=\varepsilon_1^{ir}}^{\varepsilon^{ir}} [dV^v_{iso}]_{(\tau)} \cdot [r(\varepsilon^{ir})]^{(\varepsilon^{ir}-\tau)} \quad (11)$$

where $[r(\varepsilon^{ir})]^{(\varepsilon^{ir}-\tau)}$ is the decay function; and $r(\varepsilon^{ir})$ is the parameter that decreases with ε^{ir}. Tatsuoka et al. (2002) proposed the following:

At $\varepsilon^{ir}=0$:

$$r(\varepsilon^{ir}) = r_i \text{ (positive and equal to or smaller than unity)} \quad (12a)$$

For $0<\varepsilon^{ir}\leq c$:

$$r(\varepsilon^{ir}) = \frac{r_i+r_f}{2} + \frac{r_i-r_f}{2} \cdot \cos\left[\pi \cdot \left(\frac{\varepsilon^{ir}}{c}\right)^n\right] \quad (12b)$$

For $\varepsilon^{ir}>c$:

$$r(\varepsilon^{ir}) = r_f \text{ (positive and smaller than } r_i) \quad (12c)$$

where: r_i, r_f, c and n are material constants. When $r(\varepsilon^{ir}) \equiv r_i \equiv r_f$ is constant and lower than unity, Eq. (11) returns to Eq. (10).

Combined viscosity: V^v consists of the isotach and general TESRA viscous components as:

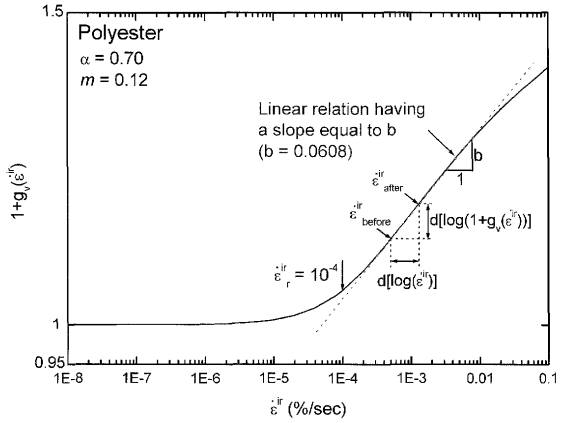

Fig. 19. Viscosity function for PET geogrid, obtained by Eq. (8) (i.e., $g_{v1}(\dot{\varepsilon}^{ir})$), after Hirakawa et al. (2003)

$$V^v(\varepsilon^{ir}, \dot{\varepsilon}^{ir}, h_s) = \theta \cdot V^v_{iso}(\varepsilon^{ir}, \dot{\varepsilon}^{ir}) + (1-\theta) \cdot V^v_{G.TESRA}(\varepsilon^{ir}, \dot{\varepsilon}^{ir}, h_s) \quad (13)$$

where θ is the material constant between zero and unity. When θ is equal to 1.0 and 0.0, Eq. (13) returns to, respectively, Eq. (7) (the isotach viscosity) and Eq. (11) (the general TESRA viscosity). This is the most flexible type, including the three types above. Hirakawa et al. (2003) showed that this type of viscosity is relevant to the PET geogrid and also used in the present study.

Determination of Model Parameters

Hirakawa et al. (2003) determined the model parameters for the combined viscosity of the PET geogrid, as shown below:

1) The parameters of the viscosity function (i.e., $g_v(\dot{\varepsilon}^{ir})$, Eq. (8)) were determined based on the measured rate-sensitivity coefficient, β, as follows. Figure 19 shows the relationship between $\log(1+g_v(\dot{\varepsilon}^{ir}))$ and $\log(\dot{\varepsilon}^{ir})$ in the full-log plot determined by Hirakawa et al. (2003):
   a) The parameters α and m were determined by trial and error so that the relationship between $\log(1+g_v(\dot{\varepsilon}^{ir}))$ and $\log(\dot{\varepsilon}^{ir})$ becomes linear for a range of $\dot{\varepsilon}^{ir}$ encountered in the test from which the β value was determined and has a slope equal to $b=\beta/\ln(10)$. This relation is obtained as follows. For a sudden change in $\dot{\varepsilon}^{ir}$ from $(\dot{\varepsilon}^{ir})_{before}$ to $(\dot{\varepsilon}^{ir})_{after}$, as depicted in Fig. 19, we obtain:

$$d[\log(1+g_v(\dot{\varepsilon}^{ir}))] = b \cdot \log\{(\dot{\varepsilon}^{ir})_{after}/(\dot{\varepsilon}^{ir})_{before}\} \quad (14a)$$

$$d[\ln(1+g_v(\dot{\varepsilon}^{ir}))] = b \cdot \ln\{(\dot{\varepsilon}^{ir})_{after}/(\dot{\varepsilon}^{ir})_{before}\} \quad (14b)$$

The data presented in Fig. 17 were obtained from the behaviour immediately after a step change in the strain rate, for which the increment $d\varepsilon^{ir}$ is negligible and a meaningful decay in the viscous load component has not yet started. So, irrespective of the viscosity type for the test material, the following equation is obtained by substituting the equations for the isotach viscosi-

ty, $V=V^f\cdot\{1+g_v(\dot{\varepsilon}^{ir})\}$ and $\Delta V^v=\Delta[V^f\cdot g_v(\dot{\varepsilon}^{ir})]$ $=V^f\cdot d[g_v(\dot{\varepsilon}^{ir})]$, into Eq. (6):

$$\frac{V^f\cdot d[g_v(\dot{\varepsilon}^{ir})]}{V^f\cdot[1+g_v(\dot{\varepsilon}^{ir})]}=d[\ln(1+g_v(\dot{\varepsilon}^{ir}))]$$

$$=\beta\cdot\log\{(\dot{\varepsilon}^{ir})_{after}/(\dot{\varepsilon}^{ir})_{before}\} \quad (15)$$

By comparing Eqs. (14b) and (15), we obtain the relation that $\beta=b\cdot\ln 10$. The values, $\alpha=0.70$ and $m=0.12$, were thus determined, which provide $b=0.0608$ and thus $\beta=0.1400$, which is nearly the same as the measured one ($=0.1428$). It is to be noted that this linear portion cannot be extended to a zone where $\dot{\varepsilon}^{ir}$ is smaller than some lower limit. This is because, if this linear portion were valid when $\dot{\varepsilon}^{ir}$ approaches zero, the value of $g_v(\dot{\varepsilon}^{ir})$ becomes negative and ultimately negatively infinitive when $\dot{\varepsilon}^{ir}$ becomes zero. In reality, the value of $g_v(\dot{\varepsilon}^{ir})$ becomes zero as $\dot{\varepsilon}^{ir}$ becomes zero. Therefore, the introduction of this non-linear part in the range of $\dot{\varepsilon}^{ir}$ lower than some limit into the $\log(1+g_v(\dot{\varepsilon}^{ir}))$ and $\log(\dot{\varepsilon}^{ir})$ relation of the viscosity function, $g_{v1}(\dot{\varepsilon}^{ir})$, as shown in Fig. 19, is necessary. It can be shown that the parameters, b and β, and the parameters of Eq. (9) are linked as $\beta=b\cdot\ln 10=\alpha^*\cdot(1+b^*)\cdot\ln 10$.

b) The parameter $\dot{\varepsilon}_r^{ir}$ of Eq. (8) does not control the slope b of the linear part of the $\log(1+g_v(\dot{\varepsilon}^{ir}))$ and $\log(\dot{\varepsilon}^{ir})$ relation, but it shifts the curve laterally in the plot shown in Fig. 19. That is, the $\dot{\varepsilon}_r^{ir}$ value is the value of $\dot{\varepsilon}^{ir}$ where the $\log(1+g_v(\dot{\varepsilon}^{ir}))$ and $\log(\dot{\varepsilon}^{ir})$ relation becomes non-linear as $\dot{\varepsilon}^{ir}$ decreases, and the value of $g_v(\dot{\varepsilon}^{ir})$ increases with a decrease in the value of $\dot{\varepsilon}_r^{ir}$ under otherwise the same conditions. The value $\dot{\varepsilon}_r^{ir}=10^{-4}\%/\text{sec}$ was determined so that all the observed rate-dependent behaviours (i.e., observed creep strain rates and load relaxation rates for different initial strain rates and at different load levels; ML curves at different constant strain rates and with step changes) obtained by Hirakawa et al. (2003) can be well simulated when based on the reference relation that had been determined for the respective test.

2) The parameters r_i, r_f, c and n of the decay function (Eq. (12)) as well as the combined parameter, θ (Eq. (13)) were also determined empirically so that all the observed trends of rate-dependent behaviour can be well simulated. The values $r_i=1.0$ and $r_f=0.15$ (both defined for ε^{ir} expressed in %); and $c=0.4$; and $n=0.6$ were determined by referring to the decay behaviour of tensile load-tensile strain relation observed: a) when ML continues at a constant $\dot{\varepsilon}$ after a respective step change in $\dot{\varepsilon}$; and b) after ML is restarted following sustained loading or load relaxation. The value $\theta=0.8$ was determined by referring to the observed separation between the tensile load-tensile strain curves obtained by continuous ML at different constant strain rates.

The longest period of sustained loading tests on the geogrids performed by Hirakawa et al. (2003) was only one hour. It was found that the model simulation using the model parameters together with the reference curves determined based on the data obtained by Hirakawa et al. (2003), which are shown above for PET geogrid, significantly underestimates creep strain rates observed at elapsed time much longer than one hour in the 30 day-long sustained loading tests, in particular after the creep strain rate becomes smaller than the value of $\dot{\varepsilon}_r^{ir}$ ($=10^{-4}\%$ /sec). Therefore, the following modifications were made so that both of the test results obtained by Hirakawa et al. (2003) and those from the newly performed 30 day-long sustained loading tests on PET geogrid as well as polyarylate and PVA geogrids can be simulated equally very well:

1) The values of α, m and $\dot{\varepsilon}_r^{ir}$ of the viscosity function Eq. (8) (i.e., $g_{v1}(\dot{\varepsilon}^{ir})$) for respectively PET, polyarylate and PVA geogrids were kept the same as the ones determined by Hirakawa et al. (2003) considering that the $\log\{1+g_v(\dot{\varepsilon}^{ir})\}$ and $\log(\dot{\varepsilon}^{ir})$ curve of the model for each respective geogrid still provides a sufficient linear portion having a slope of b value for the range of the encountered irreversible strain rate where the respective β values were experimentally evaluated (Fig. 20). Namely, $\alpha=0.70$; $m=0.12$ and $\dot{\varepsilon}_r^{ir}=10^{-4}\%/\text{sec}$ were selected for PET geogrid; $\alpha=0.44$; $m=0.09$ and $\dot{\varepsilon}_r^{ir}=10^{-4}\%/\text{sec}$ were for polyarylate geogrid; and, $\alpha=0.76$; $m=0.12$ and $\dot{\varepsilon}_r^{ir}=10^{-4}\%/\text{sec}$ were for PVA geogrid, respectively.
2) When the irreversible strain rate $\dot{\varepsilon}^{ir}$ becomes smaller than $\dot{\varepsilon}_r^{ir}$ ($=10^{-4}\%/\text{sec}$), the viscous load component according to the viscosity function Eq. (8) (i.e., $g_{v1}(\dot{\varepsilon}^{ir})$) approaches zero rather fast (Fig. 20), resulting into a nearly perfect stop of creep deformation. On the other hand, the data of the 30 day-long sustained loading test showed that the creep deformation continues developing even after the $\dot{\varepsilon}^{ir}$ value became smaller than this $\dot{\varepsilon}_r^{ir}$ value. It was also found that another viscosity function Eq. (9) (i.e., $g_{v2}(\dot{\varepsilon}^{ir})$) is relevant when $\dot{\varepsilon}^{ir}$ becomes smaller than $\dot{\varepsilon}_r^{ir}$, as this function provides a more gradual decrease in the viscous component in this range of small $\dot{\varepsilon}^{ir}$ (Fig. 20). To fit the viscosity function $g_{v2}(\dot{\varepsilon}^{ir})$ to the test results for $\dot{\varepsilon}^{ir}$ smaller than $\dot{\varepsilon}_r^{ir}$, the following values were chosen; $\alpha^*=0.20$, $1+b^*=0.32$ and $\dot{\varepsilon}_0^{ir}=10^{-3}\%/\text{sec}$ for PET geogrid; $\alpha^*=0.11$, $1+b^*=0.20$ and $\dot{\varepsilon}_0^{ir}=10^{-3}\%/\text{sec}$ for polyarylate geogrid; and $\alpha^*=0.23$, $1+b^*=0.25$ and $\dot{\varepsilon}_0^{ir}=10^{-3}\%/\text{sec}$ for PVA geogrid, respectively.
3) Equation (8) (i.e., $g_{v1}(\dot{\varepsilon}^{ir})$) and Eq. (9) (i.e., $g_{v2}(\dot{\varepsilon}^{ir})$) were combined to a single relation, as shown in Fig. 20, so that $g_{v1}(\dot{\varepsilon}^{ir})$ is activated when the encountered $\dot{\varepsilon}^{ir}$ value is relatively high, which is the case when stepwise changing the strain rate and during sustained loading for a short period (such as one hour); while $g_{v2}(\dot{\varepsilon}^{ir})$ is activated when the encountered $\dot{\varepsilon}^{ir}$ value becomes smaller than "$\dot{\varepsilon}_r^{ir}$ in $g_{v1}(\dot{\varepsilon}^{ir})$", which is the case at large elapsed times in a sustained

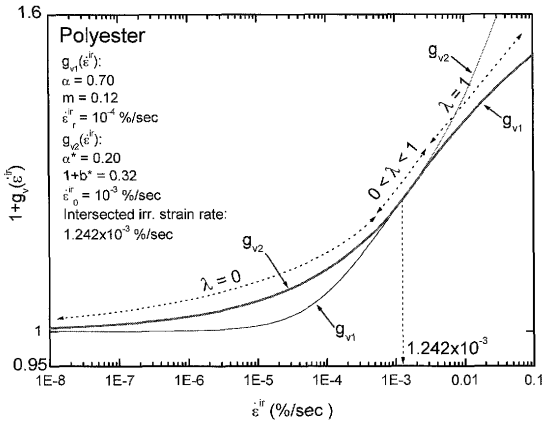

a)

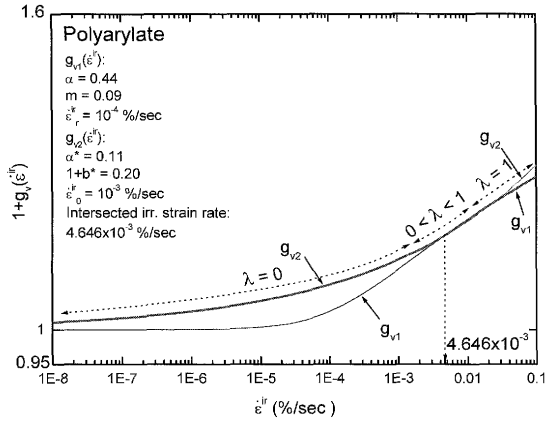

b)

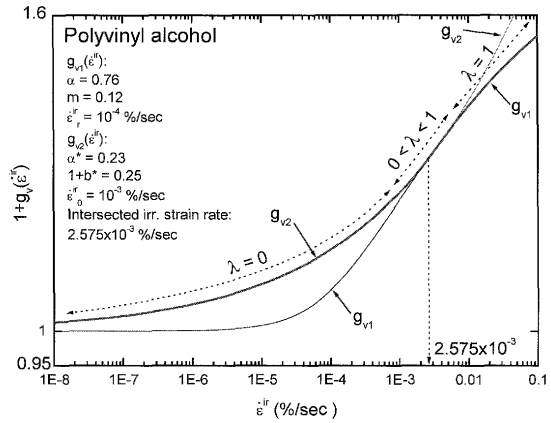

c)

Fig. 20. Combination of viscosity functions Eqs. (8) and (9) into a single relation that is relevant to a very large range of irreversible strain rate: a) PET, b) polyarylate and c) PVA geogrids

loading for a long period (e.g., 30 days). The following simplified smoothing method was employed to connect these two functions (Fig. 20):

For $\dot{\varepsilon}^{ir} \geq \sqrt{10}\cdot\dot{\varepsilon}^{ir}_{int}$:

$$g_v(\dot{\varepsilon}^{ir}) = g_{v1}(\dot{\varepsilon}^{ir}) \tag{16a}$$

For $\dot{\varepsilon}^{ir}_{int}/\sqrt{10} \leq \dot{\varepsilon}^{ir} < \sqrt{10}\cdot\dot{\varepsilon}^{ir}_{int}$:

$$g_v(\dot{\varepsilon}^{ir}) = \lambda\cdot g_{v1}(\dot{\varepsilon}^{ir}) + (1-\lambda)\cdot g_{v2}(\dot{\varepsilon}^{ir}) \tag{16b}$$

For $\dot{\varepsilon}^{ir} < \dot{\varepsilon}^{ir}_{int}/\sqrt{10}$:

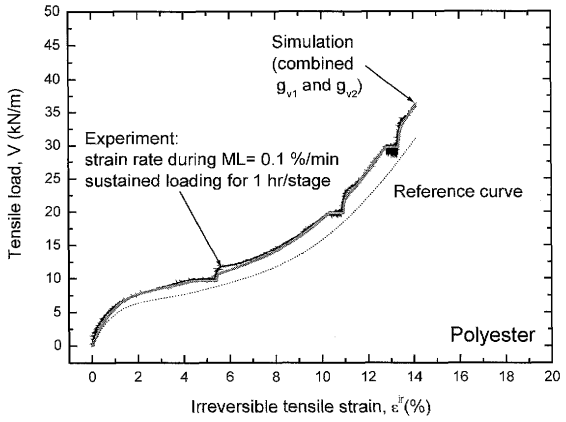

a)

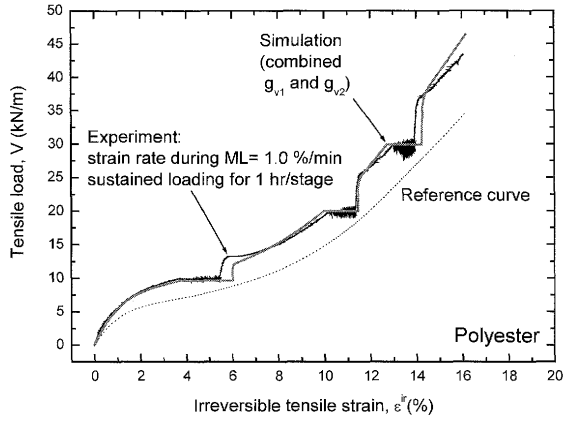

b)

Fig. 21. Simulation of the results from ML tests with sustained loading performed on PET geogrid, presented in: a) Fig. 5(a) and b) Fig. 5(b)

$$g_v(\dot{\varepsilon}^{ir}) = g_{v2}(\dot{\varepsilon}^{ir}) \tag{16c}$$

where: $\dot{\varepsilon}^{ir}_{int}$ is the irreversible strain rate where the functions $g_{v1}(\dot{\varepsilon}^{ir})$ and $g_{v2}(\dot{\varepsilon}^{ir})$ intersected each other ($=1.242\times10^{-3}$, 4.646×10^{-3} and 2.575×10^{-3}%/sec for PET, polyarylate and PVA geogrids, respectively); and $\lambda = \log(\sqrt{10}\cdot\dot{\varepsilon}^{ir}/\dot{\varepsilon}^{ir}_{int})$.

4) In the cases of PET geogrid, which exhibits the combined type of viscosity, the parameters, r_i, r_f, c and n of the decay function (Eqs. (11) and (12)) as well as the combined parameter, θ (Eq. (13)), were maintained the same as those used by Hirakawa et al. (2003).
5) The model parameters for the elastic property were kept the same as those used by Hirakawa et al. (2003).

Simulation of Test Results

The test results for PET geogrid obtained by Hirakawa et al. (2003) were re-simulated. Subsequently, the results from the 30 day-long sustained loading test were simulated for all types of geogrid performed in the present study. Note that all simulations presented below were performed by using the newly defined viscosity function (Eq. (16)). In so doing, slightly different references relations were fitted to the result from the respective test to

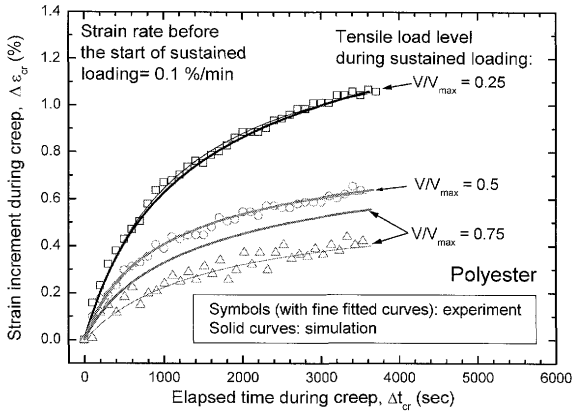

a)

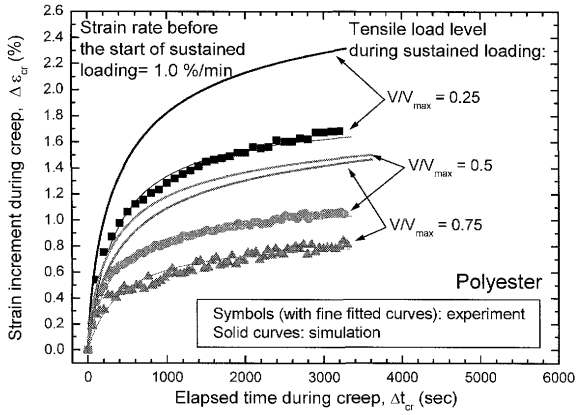

b)

Fig. 22. Simulation of time histories of creep strain from results for PET geogrid, presented in: Fig. 21(a) and b) Fig. 21(b)

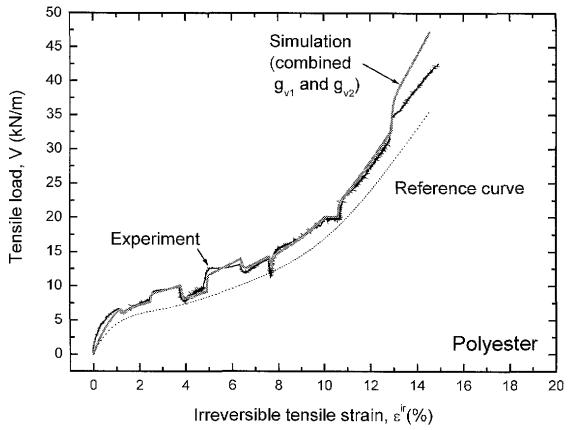

Fig. 23. Simulation of result presented in Fig. 15

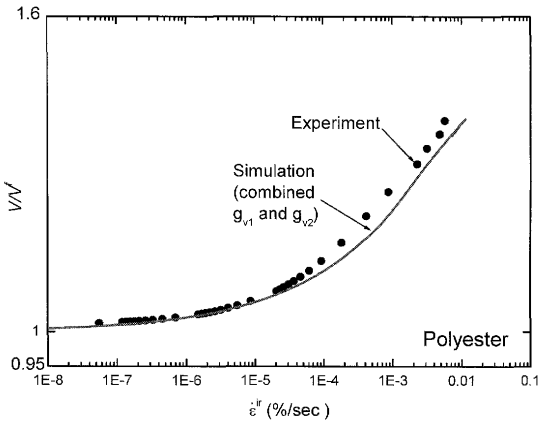

Fig. 24. Comparisons of relation between log (V/V^f) and log $(\dot{\varepsilon}^{ir})$ obtained from experiment and simulation, PET geogrid

account for an inevitable scatter in the material property among different batches of the product (e.g., Figs. 7(a) and 7(b)). This procedure was adopted to highlight the capability of the non-linear three-component model using the same parameters for elasticity as well as viscosity in simulating the rate-dependency of the tensile load and tensile strain behaviour of polymer geosynthetic reinforcement.

Figures 21(a) and 21(b) show the simulation of the results from the ML tests including multi sustained loading stages during otherwise ML at constant strain rates of 0.1%/min and 1.0%/min, respectively, for PET geogrid, presented in Figs. 5(a) and 5(b). The respective reference curve is also presented in each figure. Figures 22(a) and 22(b) show the simulation of the time histories of creep strain increment for different initial strain rate and different load levels. The initial creep strain rate (i.e., the initial irreversible strain rate) at the start of sustained loading in the respective simulation was equal to the irreversible strain rate during ML immediately before the start of the respective sustained loading. It may be seen from these figures that the proposed model can simulate rather accurately all the observed aspects of the rate-dependency of tensile load-tensile strain behaviour of the tested geosynthetic reinforcement (i.e., the creep behaviour and the stress-strain behaviour after the restart of ML at a constant strain rate following sustained loading). In particular, such peculiar observed behaviour that the creep strain becomes smaller with an increase in the load level under otherwise the same conditions is well simulated. The observation that the creep strain increases with an increase in the total strain rate during ML immediately before the start of sustained loading is also appropriately simulated.

Figure 23 shows the simulation of the result from the test in which the strain rate was changed stepwise, and sustained loading and load relaxation were performed during otherwise ML at a constant strain rate, for PET geogrid, presented in Fig. 15. It may also be seen that the proposed model can simulate rather accurately the whole aspects of the rate-dependency of the load-strain behaviour of the tested geosynthetic reinforcement when subjected to a wide variety of loading history applied in this test.

Figure 24 compares the measured and simulated relationships between the ratio of the measured V value to the corresponding V^f value obtained based on the respective reference relation and the $\dot{\varepsilon}^{ir}$ value during the 30 day-sustained loading of PET geogrid (in full-log scale). In general, the agreement between the simulation and the experiment is good. This confirms that the technique by combining the $g_{v1}(\dot{\varepsilon}^{ir})$ and $g_{v2}(\dot{\varepsilon}^{ir})$ together

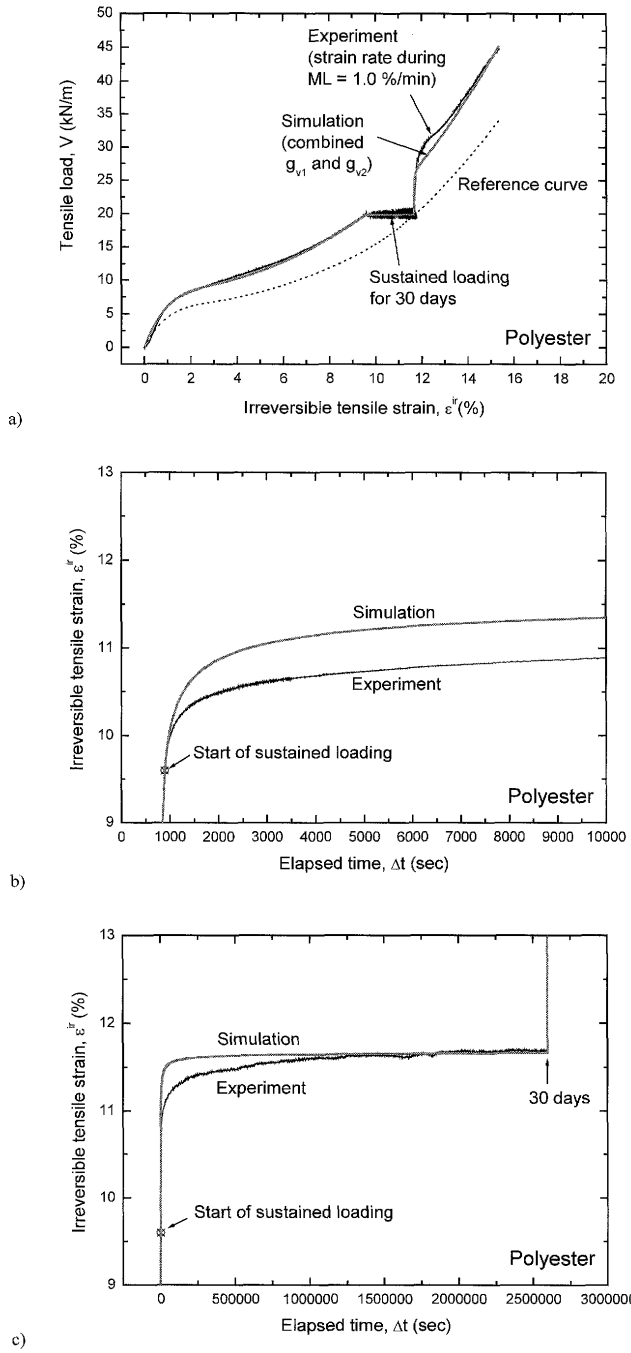

Fig. 25. Simulation of the results from the 30 day-long sustained loading test presented in Figs. 7 and 11, PET geogrid

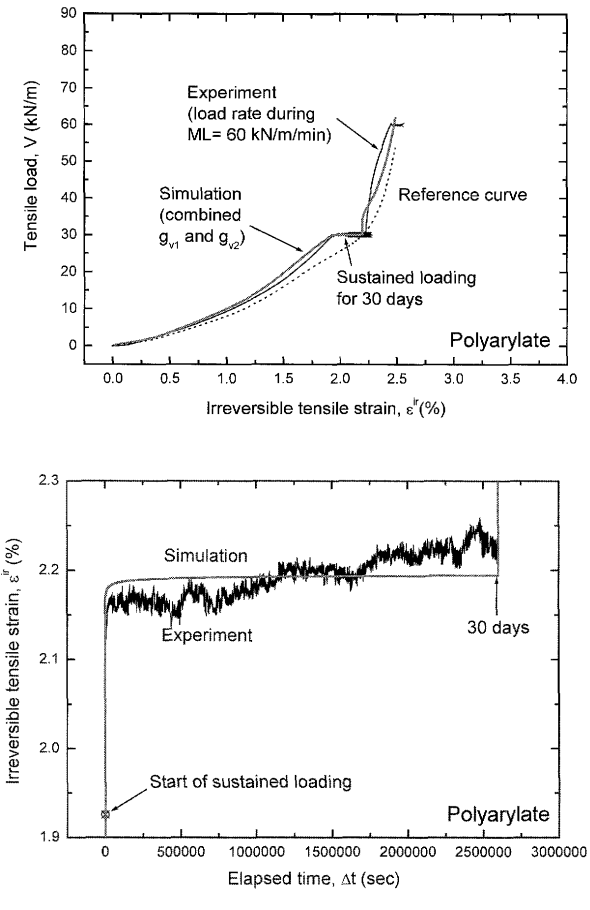

Fig. 26. Simulation of the results from the 30 day-long sustained loading test presented in Figs. 8 and 12, polyarylate geogrid

(i.e., Eq. (16)) to simulate the test result for a very large encountered range of strain rate is relevant. Figure 25(a) compares the simulated and measured tensile load and tensile strain relations for the ML test including a sustained loading stage for 30 days, performed on PET geogrid. Figures 25(b) and 25(c) compare the simulated and measured time histories of tensile strain during the 30 day-long sustained loading of PET geogrid. Figures 26 and 27 compare the simulated and measured results for polyarylate and PVA geogrids, respectively, similar to Fig. 25. It may be seen that the proposed model can very well simulate the whole aspects of the observed rate-dependency of tensile load-tensile strain relation, including the time history of creep strain. It should be admitted, however, that the simulation of the creep strain at the intermediate stage of the sustained loading is not very satisfactory (Figs. 25(c), 26(b) and 27(b)).

In summary, the creep deformation of polymer geosynthetic reinforcement is just a process of reduction in the irreversible strain rate with time at a fixed load, which is due to the viscous property of polymer geosynthetic reinforcement. For this reason, the creep strain for a given period of sustained loading is controlled by the initial creep strain rate at the start of sustained loading as well as the tangent modulus of the inviscid load—irreversible strain relation for a range of irreversible strain during the sustained loading. With the non-linear three-component model, which was used to simulate the load-strain-time behaviour of the tested polymer geosynthetic reinforcements for arbitrary loading histories as shown above, it is assumed that the strain rate becomes zero at the infinite time of sustained loading, and there is a lower bound of irreversible strain rate below which the effects of viscosity become negligible. Moreover, upon the restart of ML at a certain strain rate following a sustained loading stage, the tensile load-tensile strain relation tends to rejoin the original one which is obtained by continuous ML at the same strain rate. The non-linear three-component model is based on the fact that creep is not a degrading phenomenon.

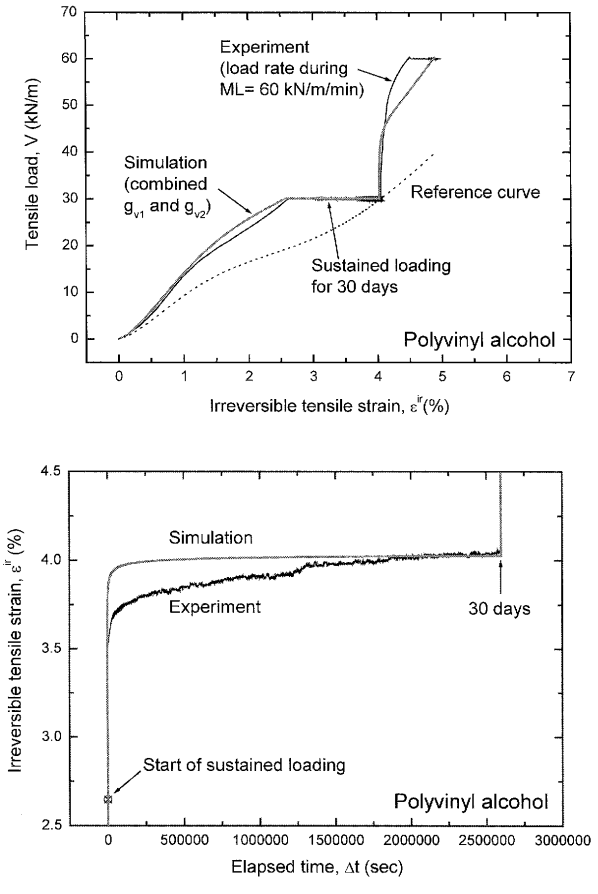

Fig. 27. Simulation of the results from the 30 day-long sustained loading test presented in Figs. 9 and 13, PVA geogrid

CONCLUSIONS

The following conclusions can be derived from the test results and simulations presented in this paper:

1) Creep deformation of the geogrids used in the present study was controlled by not only the load level but also the initial creep strain rate (i.e., the initial irreversible strain rate).
2) The tensile load-tensile strain relation immediately after the restart of monotonic loading (ML) at a constant strain rate following a sustained loading stage, including the one that lasted for 30 days, exhibited a very high stiffness, close to the elastic one. Subsequently, the load and strain relation tended to rejoin the original one that would be obtained from continuous ML test at the constant strain rate. The rupture strength was controlled by the strain rate at rupture, not affected by any pre-rupture sustained loading history. These results indicate that creep is not a degrading phenomenon while creep is actually a process of reduction in the strain rate with time, toward zero at infinite time, at constant load.
3) The proposed non-linear three-component model, which takes into account the facts described above, can simulate well all the aspects of rate-dependent load and strain behaviour of the geogrids observed in all the tests, including a wide range of loading histories, which were referred to in the paper.
4) When the creep strain history for a relatively long period, say of the order of ten years, is to be predicted by the non-linear three-component model, the model parameters should be determined by performing a relatively long sustained loading test with a controlled initial creep strain rate, as the one for 30 days performed in the present study.

ACKNOWLEDGEMENTS

This study was supported by the Japan Society for the Promotion of Science through the grant: "Advanced application of soil reinforcement technology to highly-earthquake-resistant reinforcement of existing soil structures and construction of highly-earthquake resistant and environment-friendly soil structures".

REFERENCES

1) Bathurst, R. J. and Cai, Z. (1994): In-isolation cyclic load-extension behavior of two geogrids, *Geosynthetics International*, **1**(1), 3–17.
2) Bernardi, M. and Paulson, J. (1997): Is creep a degradation phenomenon?, *Mechanically Stabilized Backfill* (ed. by Wu, J. T. H.), Balkema, 329–334.
3) Bush, D. I. (1986): Variation of long term design strength of geosynthetics in temperature, *Proc. 4th Int. Conf. Geotextiles, Geomembranes and Related Materials*, The Hague, 673–676.
4) Di Benedetto, H., Sauzéat, C. and Geoffroy, H. (1999): Modelling viscous effects for sand and behaviour in the small strain domain, *Proc. 2nd Int. Symp. Pre-failure Deformation Characteristics of Geomaterials, IS Torino* (eds. by Jamiolkowski et al.), panel presentation, Balkema, **2**, 1357–1367.
5) Di Benedetto, H., Tatsuoka, F. and Ishihara, M. (2002): Time-dependent shear deformation characteristics of sand and their constitutive modelling, *Soils and Foundations*, **42**(2), 1–22.
6) Di Benedetto, H., Tatsuoka, F., Lo Presti, D., Sauzéat, C. and Geoffroy, H. (2005): Time effects on the behaviour of geomaterials, *Deformation Characteristics of Geomaterials: Recent Investigations and Prospects* (eds. by Di Benedetto et al.), Balkema, 59–123.
7) Greenwood, J. H. (1994): Designing to residual strength of geosynthetics instead of stress-rupture, *Geosynthetics International*, **4**(1), 1–10.
8) Greenwood, J. H., Jones, C. J. F. P. and Tatsuoka, F. (2001): Residual strength and its application to design of reinforced soil in seismic areas, *Landmarks in Earth Reinforcement; Proc. Int. Symp. Earth Reinforcement* (eds. by Ochiai et al.), Balkema, **1**, 37–42.
9) Hirakawa, D., Uchimura, T., Shibata, Y. and Tatsuoka, F. (2002): Time-dependant deformation of geosynthetics and geosynthetic-reinforced soil structures, *Proc. 7th Int. Conf. Geosynthetics*, Nice, **4**, 1427–1430.
10) Hirakawa, D., Kongkitkul, W., Tatsuoka, F. and Uchimura, T. (2003): Time-dependent stress-strain behaviour due to viscous properties of geogrid reinforcement, *Geosynthetics International*, **10**(6), 176–199.
11) Kiyota, T. and Tatsuoka, F. (2006): Viscous property of loose sand in triaxial compression, extension and cyclic loading, *Soils and Foundations*, **46**(5), 665–684.
12) Kongkitkul, W., Hirakawa, D. and Tatsuoka, F. (2002): Viscous deformation during cyclic loading of geosynthetics reinforcement, *Proc. 7th Int. Conf. Geosynthetics*, Nice, **1**, 129–132.
13) Kongkitkul, W., Hirakawa, D., Tatsuoka, F. and Uchimura, T. (2004a): Viscous deformation of geosynthetic reinforcement under cyclic loading conditions and its model simulation, *Geosynthetics International*, **11**(2), 73–99.

14) Kongkitkul, W., Hirakawa, D., Uchimura, T. and Tatsuoka, F. (2004b): Loading rate effects due to viscous property on the strength and deformation property of geosynthetic reinforcement, *Proc. 3rd European Geosynthetics Conf. (EuroGeo 3)*, Munich, **2**, 533–538.
15) Kongkitkul, W., Hirakawa, D., Uchimura, T. and Tatsuoka, F. (2004c): Residual deformation due to the viscous property during cyclic loading of geosynthetic reinforcements, *Proc. 3rd Asian Reg. Conf. Geosynthetics (GeoAsia 2004)*, Seoul, 988–995.
16) Kongkitkul, W., Hirakawa, D. and Tatsuoka, F. (2005): Behaviour of geogrid-reinforced sand subject to sustained loading in PSC, *Geosynthetics and Geosynthetic-Engineered Soil Structures; Contributions from the Symposium Honoring Prof. Robert M. Koerner* (eds. by Ling et al.), McMat2005, Baton Rouge, Louisiana, USA, 251–280.
17) Leshchinsky, D., Dechasakulsom, M., Kaliakin, V. N. and Ling, H.-I. (1997): Creep and stress relaxation of geogrids, *Geosynthetics International*, **4**(5), 463–479.
18) Matsushita, M., Tatsuoka, F., Koseki, J., Cazacliu, B., Di Benedetto, H. and Yasin, S. J. M. (1999): Time effects on the pre-peak deformation properties of sands, *Proc. 2nd Int. Conf. Pre-Failure Deformation Characteristics of Geomaterials, IS Torino '99* (eds. by Jamiolkowski et al.), Balkema, **1**, 681–689.
19) Min, Y., Leshchinsky, D., Ling, H.-I. and Kaliakin, V. N. (1995): Effects of sustained and repeated tensile loads on geogrid embedded in sand, *Geotech. Test. J.*, **18**(2), 204–225.
20) Onodera, S., Fukuda, N. and Nakane, A. (2004): Long-term behavior of geogrid reinforced soil walls, *Proc. 3rd Asian Reg. Conf. Geosynthetics (GeoAsia 2004)*, Seoul, 259-264.
21) Santucci de Magistris, F., Koseki, J., Amaya, M., Hamaya, S., Sato, T. and Tatsuoka, F. (1999): A triaxial testing system to evaluate stress-strain behaviour of soils for wide range of strain and strain rate, *Geotech. Test. J.*, **22**(1), 44–60.
22) Shinoda, M., Horii, K., Bathurst, R. and Tatsuoka, F. (2002): Investigation of tensile strength after creep and stress relaxation of geogrids, *Proc. 37th Jpn. Nat. Conf. Geotech. Engrg., Japanese Geotechnical Society*, Osaka, 773–774 (in Japanese).
23) Shinoda, M., Uchimura, T. and Tatsuoka, F. (2003): Increasing the stiffness of mechanically reinforced backfill by preloading and prestressing, *Soils and Foundations*, **43**(2), 75–92.
24) Shinoda, M. and Bathurst, R. J. (2004a): Lateral and axial deformation of PP, HDPE and PET geogrids under tensile load, *Geotextiles and Geomembranes*, **22**, 205–222.
25) Shinoda, M. and Bathurst, R. J. (2004b): Strain measurement of geogrids using a video-extensometer technique, *Geotech. Test. J.*, **27**(5), 456–463.
26) Siddiquee, M. S. A., Tatsuoka, F. and Tanaka, T. (2006): FEM simulation of the viscous effects on the stress-strain behaviour of sand in plane strain compression, *Soils and Foundations*, **46**(1), 99–108.
27) Tatsuoka, F., Sato, T., Park, C.-S., Kim, Y.-S., Mukabi, J. N. and Kohata, Y. (1994): Measurements of elastic properties of geomaterials in laboratory compression tests, *Geotech. Test. J.*, **17**(1), 80–94.
28) Tatsuoka, F., Santucci de Magistris, F., Momoya, F. and Maruyama, N. (1999): Isotach behaviour and its modelling, *Proc. 2nd Int. Conf. Pre-failure Deformation Characteristics of Geomaterials, Torino, 1999* (eds. by Jamiolkowski et al.), Balkema, **1**, 491–499.
29) Tatsuoka, F., Ishihara, M., Di Benedetto, H. and Kuwano, R. (2002): Time-dependent deformation characteristics of geomaterials and their simulation, *Soils and Foundations*, **42**(2), 106–132.
30) Tatsuoka, F., Hirakawa, D., Shinoda, M., Kongkitkul, W. and Uchimura, T. (2004): An old but new issue; viscous properties of polymer geosynthetic reinforcement and geosynthetic-reinforced soil structures, Keynote Lecture, *Proc. 3rd Asian Reg. Conf. Geosynthetics (GeoAsia 2004)*, Seoul, 29–77.
31) Tatsuoka, F. (2005): Effects of viscous properties and ageing on the stress-strain behaviour of geomaterials, *Geomechanics: Testing, Modelling, and Simulation; Proc. 1st Japan-U.S. Workshop on Testing, Modelling, and Simulation* (eds. by Yamamuro and Koseki), ASCE Geotechnical Special Publication, (143), 1–60.
32) Thornton, J. S., Paulson, J. N. and Sandri, D. (1998): The stepped isothermal method for time-temperature superposition and its application to creep data on polyester yarn, *Proc. 6th Int. Conf. Geosynthetics*, Atlanta, USA, **2**, 699–706.
33) Voskamp, W., Van Vliet, F. and Retzlaff, J. (2001): Residual strength of PET after more than 12 years creep loading, *Landmarks in Earth Reinforcement; Proc. of the Int. Symp. Earth Reinforcement* (eds. by Ochiai et al.), Balkema, **1**, 165–170.